Integrated spatial genomics reveals global architecture of single nuclei

https://doi.org/10.1038/s41586-020-03126-2

Received: 1 April 2020

Accepted: 16 December 2020

Yodai Takei[1], Jina Yun[1], Shiwei Zheng[2,4], Noah Ollikainen[1], Nico Pierson[1], Jonathan White[1], Sheel Shah[1], Julian Thomassie[1], Shengbao Suo[2,4], Chee-Huat Linus Eng[3], Mitchell Guttman[1], Guo-Cheng Yuan[2,4] & Long Cai[1]✉

Identifying the relationships between chromosome structures, nuclear bodies, chromatin states and gene expression is an overarching goal of nuclear-organization studies[1–4]. Because individual cells appear to be highly variable at all these levels[5], it is essential to map different modalities in the same cells. Here we report the imaging of 3,660 chromosomal loci in single mouse embryonic stem (ES) cells using DNA seqFISH+, along with 17 chromatin marks and subnuclear structures by sequential immunofluorescence and the expression profile of 70 RNAs. Many loci were invariably associated with immunofluorescence marks in single mouse ES cells. These loci form ‘fixed points’ in the nuclear organizations of single cells and often appear on the surfaces of nuclear bodies and zones defined by combinatorial chromatin marks. Furthermore, highly expressed genes appear to be pre-positioned to active nuclear zones, independent of bursting dynamics in single cells. Our analysis also uncovered several distinct mouse ES cell subpopulations with characteristic combinatorial chromatin states. Using clonal analysis, we show that the global levels of some chromatin marks, such as H3 trimethylation at lysine 27 (H3K27me3) and macroH2A1 (mH2A1), are heritable over at least 3–4 generations, whereas other marks fluctuate on a faster time scale. This seqFISH+-based spatial multimodal approach can be used to explore nuclear organization and cell states in diverse biological systems.

The main approaches to examine nuclear organization have been sequencing-based genomics and microscopy[1,3]. Genomics approaches, such as Hi-C[6] and SPRITE[7], have been powerful in mapping interactions between chromosomes across the genome and have been scaled down to the single-cell level[1,3]. However, reconstructing 3D structures from the measured interactions relies on computational models, and it is difficult to integrate multiple modalities of measurements[2,4], including chromosome structures, in the same cells. However, microscopy-based methods can directly image chromosomes and nuclear bodies[1,3]. Recently reported methods[8–15] using Oligopaint[16] and sequential DNA fluorescence in situ hybridization (DNA FISH) have enabled imaging of many DNA loci in single cells. These studies have shown that chromosome organization is highly heterogeneous at the single-cell level[8–15], such as in the variability of chromosome folding even between two alleles in single cells[8–10,12,15]. To further discover organizational principles at the single-cell level, we need integrated tools to image chromosomes as well as nuclear bodies and chromatin marks that are aligned precisely in the same cells.

DNA seqFISH+ imaging in single cells

Building on seqFISH[17–21] and other multiplexed FISH methods[8–11,13,16,22], we have developed DNA seqFISH+ to target 3,660 loci in single mouse ES cells (Fig. 1, Extended Data Fig. 1, 2, Supplementary Table 1, 2). In two of the fluorescent channels, we used a seqFISH+ coding scheme (Methods) to target 1,267 loci approximately 2 Mb apart (Fig. 1b, c) and 1,193 loci at the 5′ end of genes. Together, these two channels labelled 2,460 loci spaced approximately 1 Mb apart across the whole genome. The third fluorescent channel targeted 60 consecutive loci at 25-kb resolution on each of the 20 chromosomes for an additional 1,200 loci (Fig. 1b, d). These approaches enabled us to examine nuclei at both 1-Mb resolution for the entire genome, and 25-kb resolution for 20 distinct regions that are at least 1.5 Mb in size (Fig. 1e).

DNA seqFISH+ detected 5,616.5 ± 1,551.4 (median ± s.d.) dots per cell in total, with 1-Mb and 25-kb resolution data (Extended Data Fig. 2h–k) in 446 cells from two biological replicates. This corresponds to an estimated detection efficiency of at least 50% in the diploid genome considering the cell cycle phases (Methods). We also detected 14.0 ± 7.4 false-positive dots per cell (median ± s.d.), as determined by the barcodes unused in the codebook.

Imaged chromosomes in single cells showed clear physical territories for individual chromosomes and variable structures among cells and chromosomes (Fig. 1e, Extended Data Fig. 3, 4). The DNA seqFISH+ measurements were highly reproducible between biological replicates (Extended Data Fig. 2l, m), and agreed with population Hi-C[23] and SPRITE data[7] (Fig. 1f, g, Extended Data Fig. 3a–g). The genomic

---

[1]Division of Biology and Biological Engineering, California Institute of Technology, Pasadena, CA, USA. [2]Department of Biostatistics and Computational Biology, Dana-Farber Cancer Institute and Harvard T.H.Chan School of Public Health, Boston, MA, USA. [3]Division of Chemistry and Chemical Engineering, California Institute of Technology, Pasadena, CA, USA. [4]Present address: Department of Genetics and Genomic Sciences and Charles Bronfman Institute for Personalized Medicine, Icahn School of Medicine at Mount Sinai, New York, NY, USA. ✉e-mail: lcai@caltech.edu

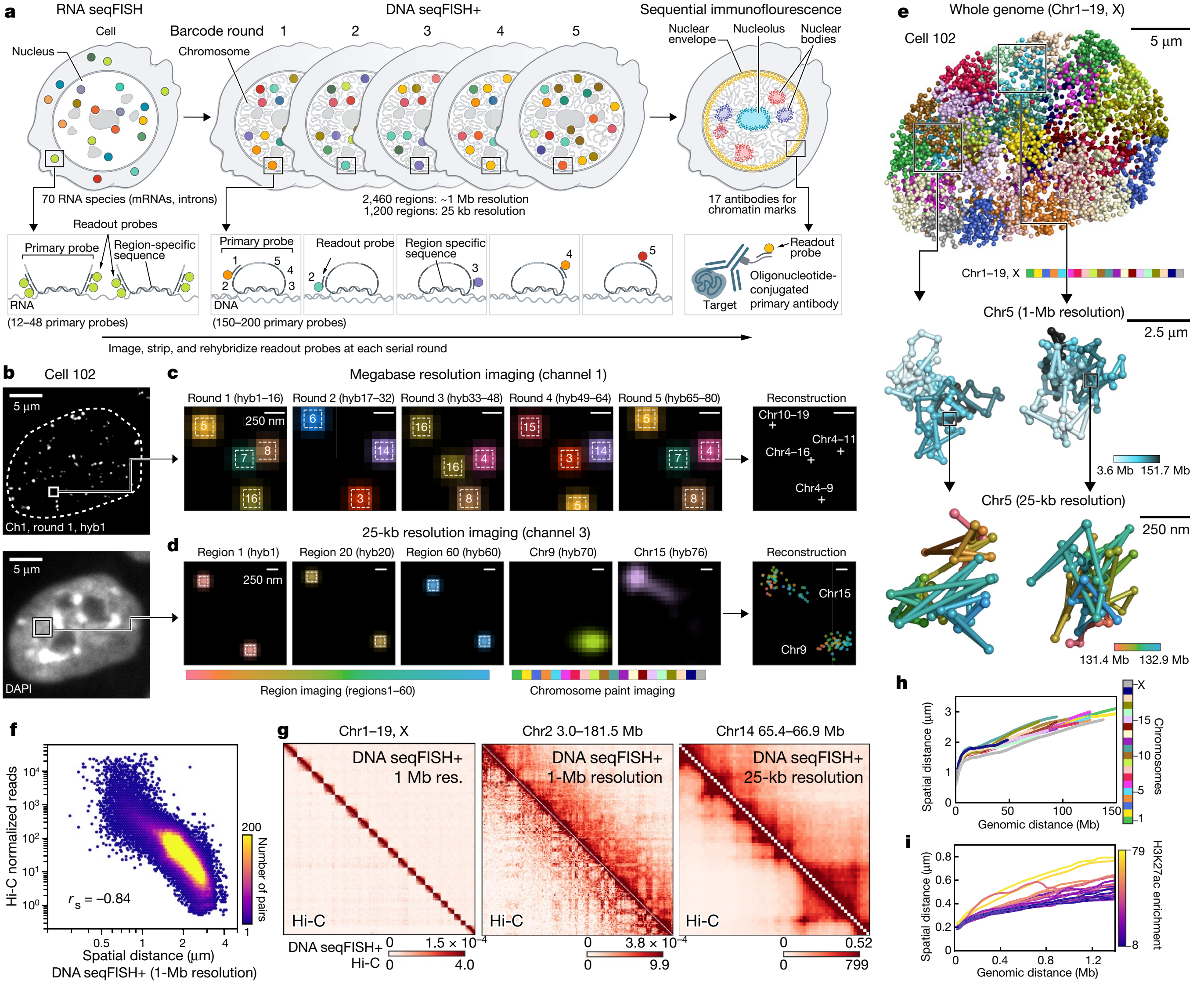

Fig. 1 | DNA seqFISH+ imaging of chromosomes. a, Schematic for DNA seqFISH+ combined with RNA seqFISH and sequential immunofluorescence (Methods). **b**, Example images of DNA seqFISH+ in a mouse ES cell. Top, DNA seqFISH+ image from one round of hybridization (hyb1) in a single *z*-section. Bottom, DAPI image of the same *z*-section of the cell. Ch, channel. **c**, Zoomed-in view of the boxed region in **b** through five rounds of barcoding. Images from 16 serial hybridizations are collapsed into a single composite image, corresponding to one barcoding round. White boxes on pseudocolour spots indicate identified barcodes. **d**, Zoomed-in view of the boxed region in **b** through 60 rounds targeting adjacent regions at 25-kb resolution followed by 20 rounds of chromosome (chr) painting in channel 3. Scale bars, 250 nm (**c**, **d**). **e**, Three-dimensional reconstruction of a single mouse ES cell nucleus. Top, individual chromosomes labelled in different colours. Middle, two alleles of chromosome 5 coloured on the basis of chromosome coordinates. Bottom, two alleles of 1.5-Mb regions in chromosome 5 with 25-kb resolution. **f**, Comparison of median spatial distance between pairs of intra-chromosomal loci by DNA seqFISH+ and Hi-C[23] frequencies. Spearman correlation coefficient of −0.84 computed from $n = 146{,}741$ unique intra-chromosomal pairs in autosomes. **g**, Concordance between DNA seqFISH+ (top right) and Hi-C[23] maps (bottom left) at different length scales. **h**, **i**, Physical distance as a function of genomic distance at 1-Mb resolution (**h**) and 25-kb resolution (**i**). Median spatial distance per genomic bin are shown. In **i**, H3K27ac enrichments of the entire region are obtained from ChIP–seq[24]. $n = 446$ cells in 2 biological replicates (**f**–**i**).

distance versus physical distance scaling relationships for each chromosome differ among the chromosomes at 1-Mb resolution as well as at 25-kb resolution (Fig. 1h, i, Extended Data Fig. 4c, d), showing that regions with low H3 lysine 27 acetylation (H3K27ac) marks[24] tend to have more compact spatial organization (Fig. 1i), possibly owing to different underlying epigenetic states[25].

Integrated measurements in single cells

We integrated our analysis of the genome (DNA seqFISH+) with the transcripts (RNA seqFISH) as well as histone modifications and subnuclear structures (sequential immunofluorescence) (Fig. 1a, Extended Data Fig. 1a). Seventeen primary antibodies targeting nuclear lamina[26], nuclear speckle[27], nucleolus[28] and active and repressive histone modification markers[29] were conjugated with DNA oligonucleotides[30,31], enabling the selective readout of individual primary antibodies with fluorescently labelled readout probes (Fig. 2a, Extended Data Figs. 1a, 2f, g, 5). These antibodies and RNA FISH probes for 70 messenger RNA and intron species were hybridized in the same cells as the DNA seqFISH+ probes. Additionally, four repetitive regions that relate to nuclear organization[32,33] were sequentially imaged with DNA FISH (Extended Data Fig. 5a).

We extensively optimized the combined protocols (Extended Data Fig. 1a, 2a–g, Methods) to profile these different modalities and

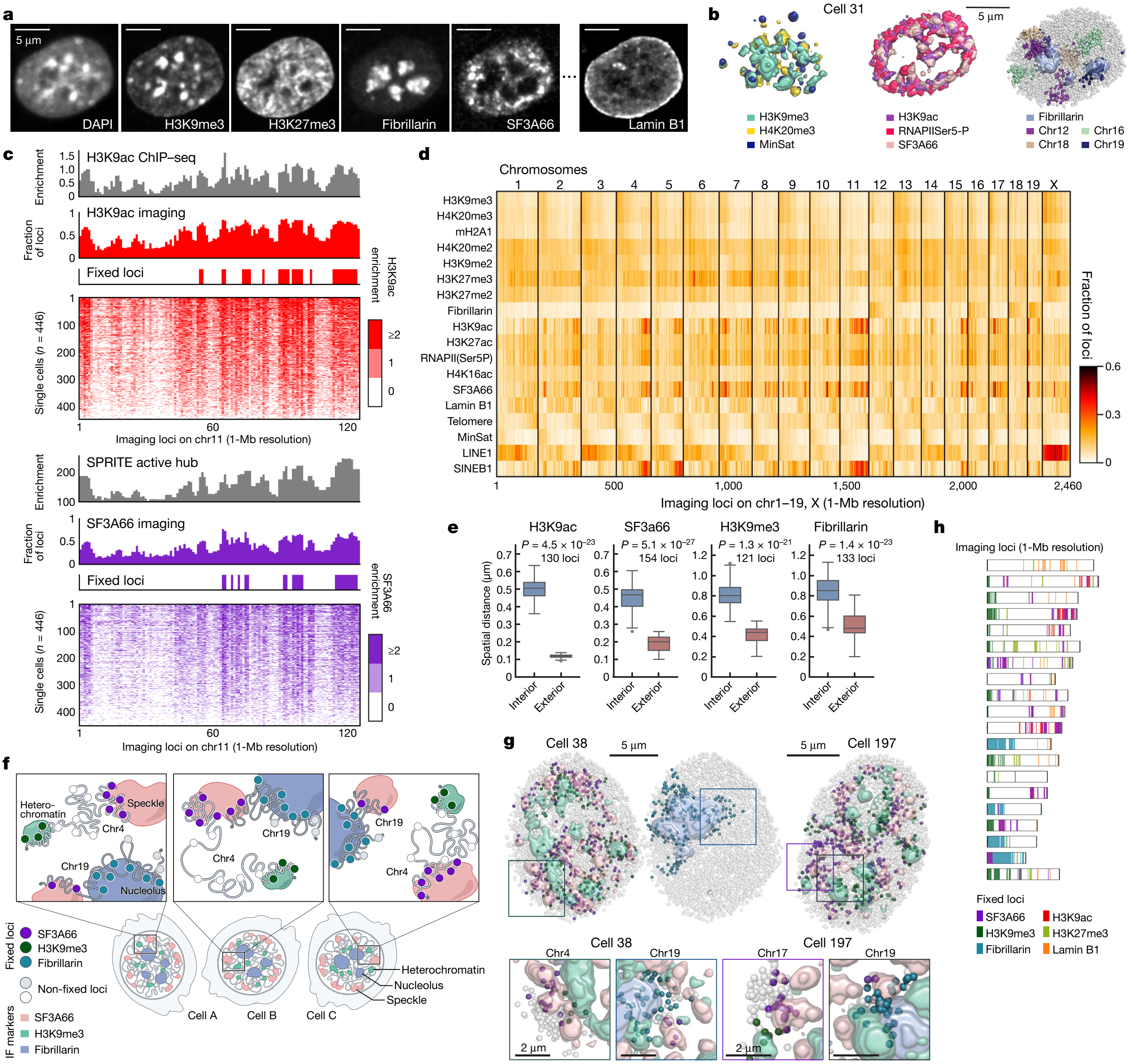

Fig. 2 | DNA seqFISH+ combined with sequential immunofluorescence reveals invariant features. **a**, DAPI and immunostaining in a mouse ES cell nucleus. Scale bars, 5 µm. **b**, Three-dimensional reconstruction of sequential immunofluorescence and DNA seqFISH+ of the cell in **a**. Immunofluorescence pixels with intensity *Z*-score values above 2 are shown (for other markers and cells, see Extended Data Fig. 5c, d). **c**, Comparison of chromatin profiles—the fraction of loci found within 300 nm of H3K9ac and SF3A66 exteriors—with corresponding reference profiles[7,24] (top) and the single-cell spatial proximity profiles of 446 single cells sorted by enrichment (bottom). Fixed loci were determined by *Z*-score above 2 from loci in all chromosomes. **d**, Heat map showing fraction of DNA loci within 300 nm from interiors of immunofluorescence markers and repetitive elements at 1-Mb resolution (see Extended Data Fig. 5g for 25-kb resolution data). **e**, Comparison of median distance of fixed loci to immunofluorescence interior and exterior voxels (Methods). *P* values by two-sided Wilcoxon's signed rank-sum test. In box plots, the centre line represents the median, boxes show the interquartile range, whiskers show values within 1.5 times the interquartile range and points represent outliers. **f**, Illustration showing chromosome 4 with fixed loci for SF3A66 and H3K9me3, whereas chromosome 19 contains fixed loci for SF3A66 and fibrillarin. IF, immunofluorescence. **g**, Top, representative 3D images for fixed loci and immunofluorescence markers. For immunofluorescence marks, pixels with intensity *Z*-score values above 2 for each immunofluorescence mark are shown. Bottom, zoomed-in views of individual chromosomes (chr4, chr17 or chr19) and three markers (SF3A66, H3K9me3 and fibrillarin), For other chromosomes, markers and cells, see Extended Data Fig. 6h, i. **h**, Fixed distribution of loci along the chromosome coordinates for all chromosomes. Each bin represents an imaging locus from 1-Mb resolution DNA seqFISH+ ($n = 2,460$ loci). $n = 446$ cells from 2 biological replicates (**c**–**h**).

accurately align between immunofluorescence and DNA FISH images for more than 130 rounds of hybridizations on an automated confocal microscope.

Repressive histone marks (for example, H3K9me3 and H4K20me3) colocalized with DAPI-rich regions and minor satellite DNA (MinSat) corresponded to pericentromeric and centromeric heterochromatin[32,33] (Fig. 2b left, Extended Data Fig. 5d). Immunofluorescence of RNA polymerase II phosphorylated on Ser5 (RNAPII(Ser5P)) and active marks (H3 lysine 9 acetylation (H3K9ac) and H3K27ac) localized to the periphery of nuclear speckles (SF3A66) (Fig. 2b middle, Extended Data Fig. 5d) and were excluded from both heterochromatic regions and the nuclear lamina (Extended Data Fig. 5d), consistent with previously reported localization patterns[27,34]. We also note that chromosomes 12, 16, 18 and 19, which contain ribosomal DNA repeat sequence (rDNA) arrays[7], showed significant association with the nucleoli (Fig. 2b right, Extended Data Fig. 5d).

Fixed loci are consistent in single cells

From the integrated multiplexed immunofluorescence and DNA seqFISH+ data, we systematically calculated the physical distances between each DNA locus and the nearest 'hot' immunofluorescence voxel, defined by being two s.d. above the mean value for each immunofluorescence marker (Extended Data Fig. 5b, c). Because many immunofluorescence markers form discrete globules in the nucleus, we also calculated the distance of each DNA locus from the exterior of immunofluorescent nuclear bodies (Methods), and confirmed that both metrics are highly correlated (Extended Data Fig. 5e, f).

We generated a 'chromatin profile' by counting the fraction of time each DNA locus is within 300 nm of the surface of an immunofluorescence mark (Fig. 2c, d, Extended Data Figs. 5g, 6, 7), the resolution of the diffraction-limited immunofluorescence images. Notably, these chromatin profiles were strongly correlated with chromatin immunoprecipitation with sequencing[24] (ChIP–seq), DamID[35] and SPRITE[7] datasets (Extended Data Fig. 6a, b) with Pearson correlation coefficients (PCCs) of 0.90 (H3K9ac), 0.82 (H3K27ac), 0.49 (lamin B1), 0.75 (SF3A66) and 0.77 (fibrillarin). The good agreement at 1-Mb resolution between the imaging data and the ChIP–seq data suggests that proximity to nuclear bodies may have an extensive role in regulating the chromatin states of DNA loci.

At the single-cell level, many DNA loci appear consistently close to particular immunofluorescence marks in a large percentage of cells (Fig. 2c, Extended Data Fig. 6f). For example, the locus of the *Pou5f1* (also known as *Oct4*), a master regulator of pluripotency, appeared to be close to the exterior of H3K9ac globules in 77.2% of the cells, and *Eef2*, a housekeeping gene, was close to nuclear speckles in 85.2% of the cells (Supplementary Table 3). We set a threshold of two s.d. above the mean to highlight the loci with the most consistent interactions. Those fixed loci for each immunofluorescence marker, either active nuclear marks (for example, SF3A66 and H3K9ac) or repressive marks (for example, H3 lysine 9 and lysine 27 methylation (H3K9me3 and H3K27me3)) (Fig. 2e–g, Extended Data Fig. 6g-i), consistently appeared on the exterior of the respective markers.

The presence of fixed loci for different immunofluorescence markers on the same chromosome (Fig. 2f–h, Extended Data Fig. 6h, i) further constrains the organization of the chromosomes. For example, chromosome 4 contained fixed loci associated with the heterochromatic marker H3K9me3 and fixed loci for the nuclear speckle protein SF3A66 (Fig. 2g, h, Extended Data Fig. 6i). Correspondingly, in 96.2% of cells, we observed chromosome 4 spanning heterochromatic globules and nuclear speckles (Supplementary Table 3). Each chromosome contains a unique combination of fixed immunofluorescent mark loci (Fig. 2h), and corresponds to the association between the chromosome and nuclear bodies consistently in single cells (Fig. 2g, Extended Data Fig. 6i). Previous studies[7,36,37] have explored nuclear lamina, speckle and nucleolus as deterministic scaffolds for chromosome organization. Our results extend these findings in single cells. Together, despite the variability in appearance in the single cell chromosome structures and nuclear body positioning[5], there are invariant features across multiple DNA–nuclear body associations that give rise to the organization of the nucleus in single cells.

Combinatorial marks define nuclear zones

We clustered individual binned voxels[38] on the basis of their combinatorial chromatin profiles and obtained 12 major clusters (Fig. 3a, Extended Data Fig. 8a–e). Some of these clusters or nuclear zones (Fig. 3a, b) corresponded to nuclear bodies such as the nuclear speckles[27] (zone 1) enriched with the splicing factor SF3A66, the nucleolus[28] (zones 8 and 9) enriched with fibrillarin, a key nucleolar protein. In addition, zone 2, enriched in active marks (RNAPII(Ser5P) and histone acetylation marks), formed contiguous regions in the nucleus that often surrounded the nuclear speckles[27] (Fig. 3a, b). The three heterochromatin zones (zones 5, 6 and 7) had distinct combinatorial marks (Fig. 3a). In addition, several zones showed a mixture of marks, such as zone 3 and 4 with mixed repressive and active marks (Fig. 3a). These zones form physically distinct regions in single nuclei (Fig. 3b, Extended Data Fig. 8f–h), rather than being well-mixed in the nucleus, suggesting that zones may form owing to phase separation or other mechanisms[39].

We assigned a zone for each DNA locus, or an interface if more than one zone was present (Methods). Some loci had characteristic zone associations, such as *Pou5f1*, which was associated with active zone 2 and zone 1–2 and zone 2–3 interfaces (Fig. 3b, Extended Data Fig. 8i, j, Supplementary Table 4). Many loci were enriched at interfaces between zones (Fig. 3b, c, Extended Data Fig. 8f, k, Supplementary Table 5), consistent with the observation of loci near the exterior of nuclear bodies and chromatin marks (Fig. 2e, g). For example, DNA loci are 46.3% more likely to be detected at zone 2–3 interfaces than random chance (Fig. 3c). Furthermore, pairs of interchromosomal loci were enriched at the active zone 2–3 interfaces, whereas pairs of intrachromosomal loci were enriched at the heterochromatic zone 5–7 interfaces and nucleolus zone 8–9 interfaces (Fig. 3c). Immunofluorescence images and zone assignments were limited by diffraction and background, and that even finer granularity would be observed with super-resolution imaging of the immunofluorescence markers (Methods).

Active loci are pre-positioned

Simultaneous imaging of nascent transcription active sites (TASs) by intronic FISH against 1,000 genes[20], 14 immunofluorescence markers and DAPI in the same cells showed that TASs appear at the surface, rather than the centre, of RNAPII-dense regions in the nuclei (Fig. 3d, Extended Data Fig. 8h). They also appeared in the interfaces between active and mixed zones zone 2–3 twice as frequently compared with random chance, 16.8% vs 8.0% (Fig. 3c, Extended Data Fig. 8k, Supplementary Table 5). Average expression level across 1 Mb correlated with the association with active and nuclear speckle zones and interfaces (Fig. 3f, Extended Data Fig. 8l, m), consistent with previous findings[37].

However, in single cells, we observed little correlation between mRNA and intron expression and proximity with active and speckle zones among the genes we examined (27 genes for mRNA spanning a large range of expression levels and 14 genes for intron) (Fig. 3g–j, Extended Data Fig. 8n, o). Given the typically shorter lifetime of introns and mRNAs (minutes to hours, respectively) compared with the possibly longer timescale of chromosomal positioning, it is likely that most genes are not dynamically positioned to the active zones (zones 1 and 2) for transcription. Rather, it is likely that most genes are pre-positioned to those zones or interfaces, and their positioning may be determined by underlying epigenetic states as well as other factors such as neighbouring gene density[7].

Global chromatin states are heterogeneous

Mouse ES cells have been shown to exist as metastable transcriptional states[40–42] with subpopulations of differential gene expression profiles characterized both by single-cell RNA sequencing (scRNA-seq)[42] and mRNA seqFISH (Extended Data Fig. 9a–c, Supplementary Table 6). We observed that the overall intensities of immunofluorescence signals in the nucleus also showed substantial heterogeneities among single cells (Fig. 4a). Clustering analysis of the immunofluorescence data (Fig. 4b, Extended Data Fig. 9d, e) showed at least seven distinct states

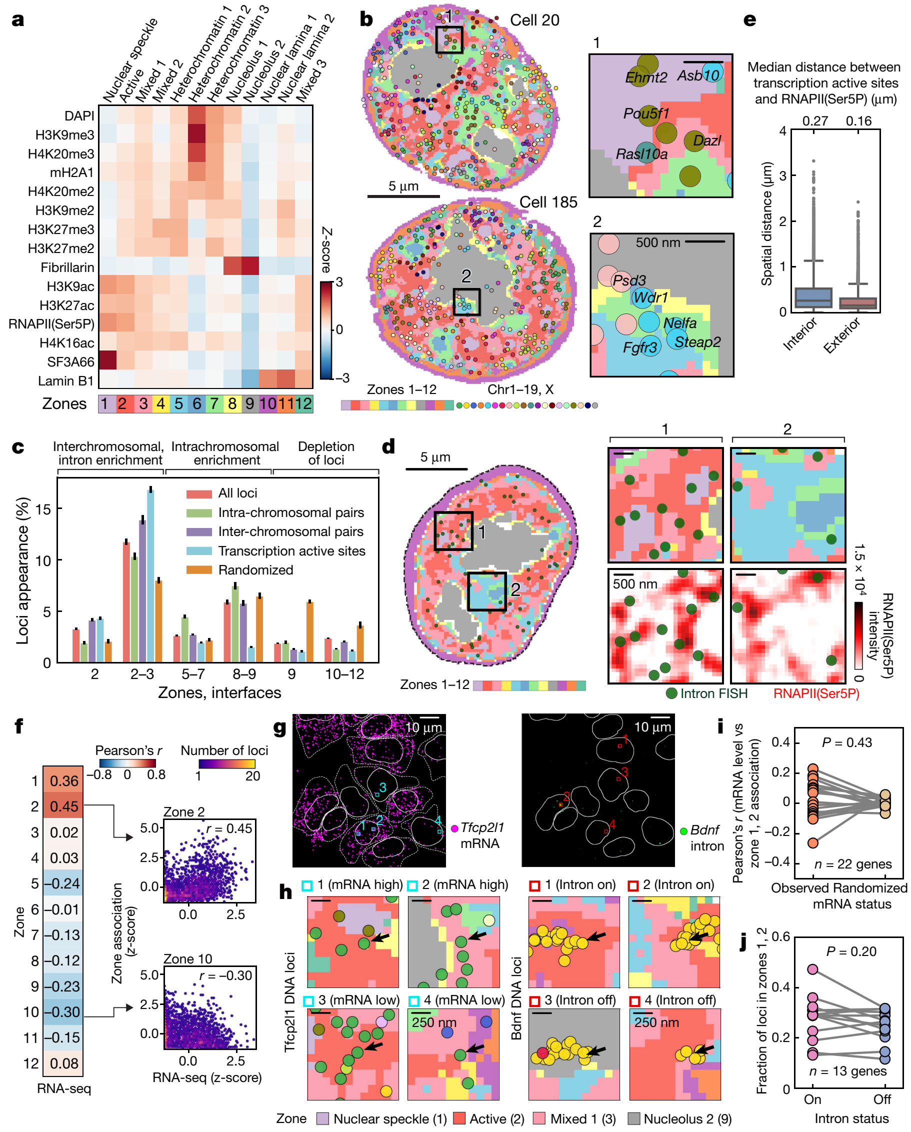

Fig. 3 | Combinatorial chromatin patterns reveal nuclear zones. **a**, Heat map for differential enrichment of individual chromatin markers in each zone. **b**, Reconstructions of nuclear zones and DNA loci in a single *z*-plane. Zoomed-in views (right) show gene loci—for example, *Pou5f1* in zone 1 or zone 1–2 interfaces (top) and loci around the nucleolus and heterochromatin zones (bottom). **c**, Frequency of DNA loci or TAS association with zones and interfaces in single cells. Data are mean values from 20 bootstrap trials ± s.e.m. **d**, Left, TAS targeted by 1,000-gene intron FISH and nuclear zones. Right, zoomed-in views show the enrichment of TAS at the interfaces of nuclear zones (top) and at the exterior of the RNAPIISer5-P staining (background-subtracted, bottom). **e**, Spatial distance from TAS to RNAPIISer5-P staining interior and exterior voxels. In box plots, the centre line represents the median, boxes show the interquartile range, whiskers show values within 1.5 times the interquartile range and points represent outliers. **f**, Pearson correlation of bulk RNA-seq[49] and zone assignment for all 1-Mb resolution loci ($n = 2{,}460$ loci). Right, density plots for individual loci. $n = 201$ cells for all DNA loci (**a**–**f**) and $n = 172$ cells for TAS (**c**–**e**), from two independent experiments. **g**, Representative maximum intensity *z*-projected RNA seqFISH images. White lines show segmented nucleus (left and right) and cytoplasm (left). **h**, Zoomed-in views from **g**, showing the zones around *Tfcp2l1* (left) and *Bdnf* DNA loci (right) with black arrows. *Tfcp2l1* is shown with 1-Mb resolution and *Bdnf* is shown with 25-kb resolution DNA seqFISH+ data. **i**, Correlation between mRNA counts of the profiled genes and their association to active zones (zones 1 and 2) in single cells. Each dot represents a gene (22 genes, $n = 125$ cells). **j**, Comparison between intron state and active zone (zones 1 and 2) association of the corresponding alleles (13 genes, $n = 125$ cells). P values by two-sided Wilcoxon's signed rank-sum test; cells in the centre field of views were used (**i**, **j**).

based on global chromatin modification levels, with most marker levels being independent from cell cycle phases (Extended Data Fig. 9f). Notably, immunofluorescence states only partially overlapped with the transcriptional states. For example, 'ground' pluripotent-state cells expressing *Zfp42*, *Nanog* and *Esrrb* as well as *Otx2*-expressing orthogonal 'primed'-state cells are present in most immunofluorescence clusters (Fig. 4b, Extended Data Fig. 9e). In addition, global levels of H3K27me3 and mH2A1 were associated with naive or ground pluripotent states whereas H3K9me3 was associated with primed pluripotent states (Extended Data Fig. 9g–j). These observations at the single-cell level extend the previous bulk studies[43,44] showing increased total H3K27me3 levels and decreased H3K9me3 heterochromatin clusters in 2i-grown naive mouse ES cells compared with serum-grown mouse ES cells.

Chromatin states persist across generations

To examine whether the heterogeneity in chromatin states, mRNA expression and chromosome organization are stable or dynamic across generations, we performed clonal analysis experiments. If clonally

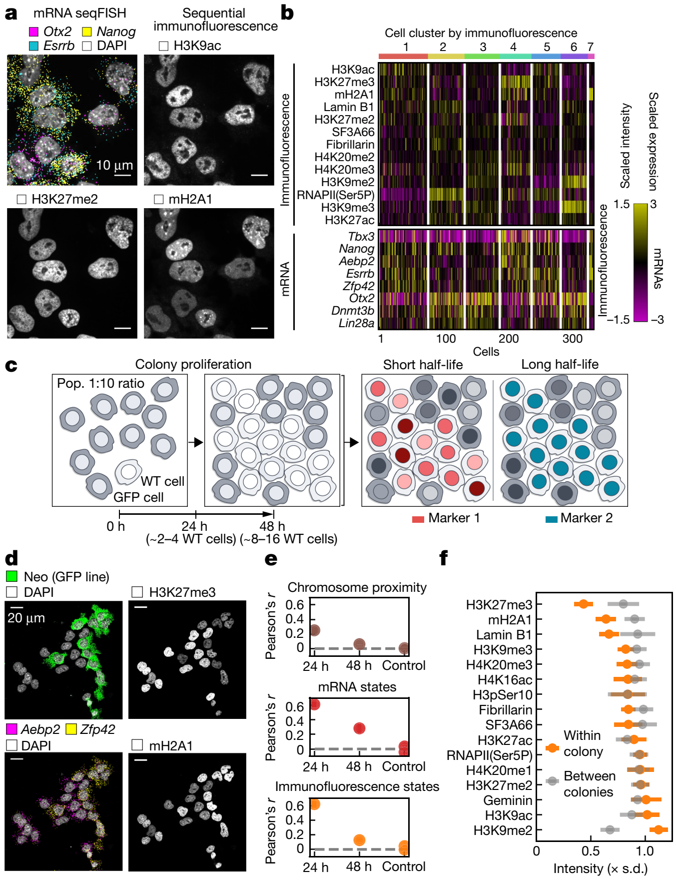

Fig. 4 | Global chromatin states are highly variable and dynamic in single cells. a, Intensities of immunofluorescence markers show heterogeneities in single cells. Images are from the same *z*-section. Scale bars, 10 μm. **b**, Heat map of cell clusters with distinct immunofluorescence profiles. Bimodally expressed *Nanog*, *Esrrb* and *Zfp42*[41] are distributed over several immunofluorescence clusters. *n* = 326 cells in the centre field of views from 2 biological replicates. **c**, Schematic of colony-tracing experiments. Intensity of markers with fast dynamics are expected to be heterogeneous within a colony. WT, wild type. **d**, Representative maximum intensity *z*-projected images for one 48-h colony, showing heterogeneities in mRNA (left) and immunofluorescence markers (right). Neo represents the neomycin resistance gene, which is expressed in a GFP cell line. Scale bars, 20 μm. **e**, Mean Pearson correlation between cells within colonies decays slowly for mRNA and chromatin states, and quickly for chromosome proximities. Control measures correlation between colonies for both 24-h and 48-h datasets. **f**, Standard deviation of individual immunofluorescence marker intensities in 48-h colonies compared with those between colonies. H3K27me3 and mH2A1 show less variance in cells within a colony (as in **d**). Data are mean values from 20 bootstrap trials ± s.e.m. (**e**, **f**). *n* = 117 unlabelled cells within colonies in 48-h dataset. *n* = 53 cells in 24-h dataset.

related cells have similar molecular states, then those states are likely to have slow dynamics, and vice versa (Fig. 4c). We seeded unlabelled mouse ES cells among GFP-positive mouse ES cells at a 1:10 ratio and cultured them for 24 or 48 h—approximately 2 and 4 generations respectively—such that each unlabelled mouse ES cell colony probably arises from a single cell (Fig. 4c, d, Extended Data Fig. 10a).

Overall mRNA and chromatin profiles were highly correlated among most cells within a colony at the 24-h time point (Fig. 4e, Extended Data Fig. 10b), and maintained some correlation even at the 48-h time point. By contrast, chromosome proximities are preserved across one cell cycle between sisters but are then rapidly lost after two generations (Fig. 4e, Extended Data Fig. 10c–e), consistent with previous studies with targeted chromosomes or regions[45–48]. Of note, the dynamics of individual immunofluorescence markers, such as mH2A1 and H3K27me3, were highly correlated within colonies but not between colonies, suggesting that these chromatin features are heritable across at least three to four generations (Fig. 4f). Conversely, many immunofluorescence marks, such as H3K9ac, did not correlate within a colony or between colonies, suggesting that these features are rapidly fluctuating.

Discussion

Our spatial multimodal approach using DNA seqFISH+ along with multiplexed immunofluorescence and RNA seqFISH enables profiling of chromosome structures, nuclear bodies, chromatin states and gene expression within the same single cells. The precisely aligned images over multiple modalities enabled us to observe invariant features across nuclei despite the heterogeneity in chromosome structures in single cells. Notably, many DNA loci, especially active gene loci, reside at the surface of nuclear bodies and zone interfaces. Functionally, localization of target loci on surfaces might suggest that regulatory factors diffuse in 2D to search for their target genes. Finally, the observation of heterogeneous and long-lived global chromatin states raises the question of whether these states have distinct pluripotency and differentiation potentials and could represent hidden variables in differentiation experiments, which warrants further investigation. We anticipate that such spatial multiomics approaches will enable further exploration of those questions in many biological contexts.

Online content

Any methods, additional references, Nature Research reporting summaries, source data, extended data, supplementary information, acknowledgements, peer review information; details of author contributions and competing interests; and statements of data and code availability are available at https://doi.org/10.1038/s41586-020-03126-2.

1. Dekker, J. et al. The 4D nucleome project. *Nature* **549**, 219–226 (2017).
2. Kelsey, G., Stegle, O. & Reik, W. Single-cell epigenomics: recording the past and predicting the future. *Science* **358**, 69–75 (2017).
3. Kempfer, R. & Pombo, A. Methods for mapping 3D chromosome architecture. *Nat. Rev. Genet.* **21**, 207–226 (2020).
4. Zhu, C., Preissl, S. & Ren, B. Single-cell multimodal omics: the power of many. *Nat. Methods* **17**, 11–14 (2020).
5. Finn, E. H. & Misteli, T. Molecular basis and biological function of variability in spatial genome organization. *Science* **365**, eaaw9498 (2019).
6. Lieberman-Aiden, E. et al. Comprehensive mapping of long-range interactions reveals folding principles of the human genome. *Science* **326**, 289–293 (2009).
7. Quinodoz, S. A. et al. Higher-order inter-chromosomal hubs shape 3D genome organization in the nucleus. *Cell* **174**, 744–757 (2018).
8. Wang, S. et al. Spatial organization of chromatin domains and compartments in single chromosomes. *Science* **353**, 598–602 (2016).
9. Bintu, B. et al. Super-resolution chromatin tracing reveals domains and cooperative interactions in single cells. *Science* **362**, eaau1783 (2018).
10. Nir, G. et al. Walking along chromosomes with super-resolution imaging, contact maps, and integrative modeling. *PLoS Genet.* **14**, e1007872 (2018).
11. Cardozo Gizzi, A. M. et al. Microscopy-based chromosome conformation capture enables simultaneous visualization of genome organization and transcription in intact organisms. *Mol. Cell* **74**, 212–222 (2019).
12. Finn, E. H. et al. Extensive heterogeneity and intrinsic variation in spatial genome organization. *Cell* **176**, 1502–1515 (2019).
13. Mateo, L. J. et al. Visualizing DNA folding and RNA in embryos at single-cell resolution. *Nature* **568**, 49–54 (2019).
14. Nguyen, H. Q. et al. 3D mapping and accelerated super-resolution imaging of the human genome using in situ sequencing. *Nat. Methods* **17**, 822–832 (2020).
15. Su, J.-H., Zheng, P., Kinrot, S. S., Bintu, B. & Zhuang, X. Genome-scale imaging of the 3d organization and transcriptional activity of chromatin. *Cell* **182**, 1641–1659 (2020).
16. Beliveau, B. J. et al. Versatile design and synthesis platform for visualizing genomes with Oligopaint FISH probes. *Proc. Natl Acad. Sci. USA* **109**, 21301–21306 (2012).
17. Lubeck, E., Coskun, A. F., Zhiyentayev, T., Ahmad, M. & Cai, L. Single-cell in situ RNA profiling by sequential hybridization. *Nat. Methods* **11**, 360–361 (2014).
18. Shah, S., Lubeck, E., Zhou, W. & Cai, L. In situ transcription profiling of single cells reveals spatial organization of cells in the mouse hippocampus. *Neuron* **92**, 342–357 (2016).
19. Takei, Y., Shah, S., Harvey, S., Qi, L. S. & Cai, L. Multiplexed dynamic imaging of genomic loci by combined CRISPR imaging and DNA sequential FISH. *Biophys. J.* **112**, 1773–1776 (2017).

20. Shah, S. et al. Dynamics and spatial genomics of the nascent transcriptome by intron seqFISH. *Cell* **174**, 363–376 (2018).
21. Eng, C. L. et al. Transcriptome-scale super-resolved imaging in tissues by RNA seqFISH+. *Nature* **568**, 235–239 (2019).
22. Chen, K. H., Boettiger, A. N., Moffitt, J. R., Wang, S. & Zhuang, X. RNA imaging. Spatially resolved, highly multiplexed RNA profiling in single cells. *Science* **348**, aaa6090 (2015).
23. Bonev, B. et al. Multiscale 3D genome rewiring during mouse neural development. *Cell* **171**, 557–572.e24 (2017).
24. Shen, Y. et al. A map of the cis-regulatory sequences in the mouse genome. *Nature* **488**, 116–120 (2012).
25. Boettiger, A. N. et al. Super-resolution imaging reveals distinct chromatin folding for different epigenetic states. *Nature* **529**, 418–422 (2016).
26. van Steensel, B. & Belmont, A. S. Lamina-associated domains: links with chromosome architecture, heterochromatin, and gene repression. *Cell* **169**, 780–791 (2017).
27. Spector, D. L. & Lamond, A. I. Nuclear speckles. *Cold Spring Harb. Perspect. Biol*. **3**, a000646 (2011).
28. Pederson, T. The nucleolus. *Cold Spring Harb. Perspect. Biol*. **3**, a000638 (2011).
29. Ludwig, C. H. & Bintu, L. Mapping chromatin modifications at the single cell level. *Development* **146**, dev170217 (2019).
30. Söderberg, O. et al. Direct observation of individual endogenous protein complexes in situ by proximity ligation. *Nat. Methods* **3**, 995–1000 (2006).
31. Agasti, S. S. et al. DNA-barcoded labeling probes for highly multiplexed Exchange-PAINT imaging. *Chem. Sci*. **8**, 3080–3091 (2017).
32. Guenatri, M., Bailly, D., Maison, C. & Almouzni, G. Mouse centric and pericentric satellite repeats form distinct functional heterochromatin. *J. Cell Biol*. **166**, 493–505 (2004).
33. Solovei, I. et al. Nuclear architecture of rod photoreceptor cells adapts to vision in mammalian evolution. *Cell* **137**, 356–368 (2009).
34. Mao, Y. S., Zhang, B. & Spector, D. L. Biogenesis and function of nuclear bodies. *Trends Genet*. **27**, 295–306 (2011).
35. Peric-Hupkes, D. et al. Molecular maps of the reorganization of genome-nuclear lamina interactions during differentiation. *Mol. Cell* **38**, 603–613 (2010).
36. Kind, J. et al. Genome-wide maps of nuclear lamina interactions in single human cells. *Cell* **163**, 134–147 (2015).
37. Chen, Y. et al. Mapping 3D genome organization relative to nuclear compartments using TSA-seq as a cytological ruler. *J. Cell Biol*. **217**, 4025–4048 (2018).
38. Gut, G., Herrmann, M. D. & Pelkmans, L. Multiplexed protein maps link subcellular organization to cellular states. *Science* **361**, eaar7042 (2018).
39. McSwiggen, D. T., Mir, M., Darzacq, X. & Tjian, R. Evaluating phase separation in live cells: diagnosis, caveats, and functional consequences. *Genes Dev*. **33**, 1619–1634 (2019).
40. Marks, H. et al. The transcriptional and epigenomic foundations of ground state pluripotency. *Cell* **149**, 590–604 (2012).
41. Singer, Z. S. et al. Dynamic heterogeneity and DNA methylation in embryonic stem cells. *Mol. Cell* **55**, 319–331 (2014).
42. Kolodziejczyk, A. A. et al. Single cell RNA-sequencing of pluripotent states unlocks modular transcriptional variation. *Cell Stem Cell* **17**, 471–485 (2015).
43. Tosolini, M. et al. Contrasting epigenetic states of heterochromatin in the different types of mouse pluripotent stem cells. *Sci. Rep*. **8**, 5776 (2018).
44. van Mierlo, G. et al. Integrative proteomic profiling reveals PRC2-dependent epigenetic crosstalk maintains ground-state pluripotency. *Cell Stem Cell* **24**, 123–137.e8 (2019).
45. Gerlich, D. et al. Global chromosome positions are transmitted through mitosis in mammalian cells. *Cell* **112**, 751–764 (2003).
46. Walter, J., Schermelleh, L., Cremer, M., Tashiro, S. & Cremer, T. Chromosome order in HeLa cells changes during mitosis and early G1, but is stably maintained during subsequent interphase stages. *J. Cell Biol*. **160**, 685–697 (2003).
47. Thomson, I., Gilchrist, S., Bickmore, W. A. & Chubb, J. R. The radial positioning of chromatin is not inherited through mitosis but is established de novo in early G1. *Curr. Biol*. **14**, 166–172 (2004).
48. Essers, J. et al. Dynamics of relative chromosome position during the cell cycle. *Mol. Biol. Cell* **16**, 769–775 (2005).
49. Hormoz, S. et al. inferring cell-state transition dynamics from lineage trees and endpoint single-cell measurements. *Cell Syst*. **3**, 419–433 (2016).

Methods

Data reporting

No statistical methods were used to predetermine sample size. The experiments were not randomized and the investigators were not blinded to allocation during experiments and outcome assessment.

DNA seqFISH+ encoding strategy

A 16-base coding scheme with 5 rounds of barcoding is used in DNA seqFISH+ for the 1-Mb resolution data in fluorescent channel 1 (643 nm) and 2 (561 nm) (Extended Data Fig. 1b, Supplementary Table 2). The first 3 rounds of barcoding codes for $16^3 = 4{,}096$ unique barcodes. Two additional rounds of parity check (linear combinations of the first three rounds) are included. A total of 2,048 barcodes were selected to correct for dropouts in any 2 out of 5 rounds of barcoding and used in both channel 1 and 2. The 16-pseudocolor base was generated by hybridizing the sample with 16 different readout oligonucleotides sequentially.

To image 20 distinct regions (1.5–2.4 Mb in size) with 25-kb resolution, a combined strategy of diffraction limited spot imaging and chromosome painting is used in channel 3 (488 nm) (Extended Data Fig. 1c, Supplementary Table 2), by extending previously demonstrated 'track first and identify later' approach[19]. For the initial 60 rounds, 25-kb regions are read out one at a time on all 20 chromosomes in each round of hybridization. These 60 rounds can resolve the 25-kb loci within each distinct region but cannot distinguish to which chromosome the loci belong. The next 20 rounds are used to resolve the identities of the 20 distinct regions or chromosomes by painting the entire region (1.5–2.4 Mb) one at one time. With this strategy, identities for 1,200 loci are decoded.

To implement these strategies, 80 unique readouts are used in each fluorescent channel for a total of 240 readouts for 3 channels.

Primary probe design

RNA seqFISH probes were designed as previously described[20,21]. In brief, 35-nt RNA target binding sequences, 15-nt unique readout probe binding sites for each RNA target, and a pair of 20-nt primer binding sites at 5′ and 3′ end of the probe for probe generation (see 'Primary probe synthesis') are concatenated. Marker genes (Supplementary Table 6) were selected based on previous single-cell imaging and RNA-seq studies in mouse ES cells[20,41,42,49].

For DNA seqFISH+ target region selection (Supplementary Table 1), the unmasked and repeat-masked GRCm38/mm10 mouse genome FASTA files were downloaded from Ensembl release 93[50]. To select target regions for channel 1, the entire mouse genome was split into candidate target regions of 25 kb. Masking coverage was evaluated for each region using the repeat-masked genome. Regions with a high percentage of masked bases were removed from consideration. Then target regions were further selected to space out approximately 2 Mb in the genome coordinates. To select target regions for channel 2, candidate genes related to mouse ES cell pluripotency and differentiation were selected from previous studies[35,42,51], and then 25-kb regions were selected by centering the transcription starting sites of the genes. To select target regions for channel 3, gene loci with various expression levels in mouse ES cells as well as gene-poor regions were initially selected as a 2.5-Mb block, and splitted into 25-kb blocks. Only a single 2.5-Mb region was selected per chromosome.

Region-specific primary probes were designed as previously described for single-stranded RNA[21] with some modifications. The target region was extracted from the unmasked genome. Probe sequences were produced by taking the reverse complement of 35-nt sections of the target region. Starting from the 5′ end of the forward strand, candidate probes were tested for viability, shifting one base at a time. Probes that contained five or more consecutive bases of the same kind, or had a GC content outside of 45–65%, were considered non-viable. Each time a viable probe was discovered, evaluation was switched to the opposite strand, starting 19 nt downstream from the start of the viable probe to mitigate cross-hybridization between neighbouring probes. This procedure was repeated until the end of the target region was reached.

Next, the probes were aligned to the unmasked mouse genome for off-target evaluation using Bowtie2[52]. Any alignment containing at least 19 matched bases that fell outside the genomic coordinates of the target region was considered off-target. Probes with more than 10 total off-target hits were dropped. Off-target hits were grouped into 100-kb bins and stored for use in the final probe selection. Bins were overlapped by 50 kb so that closely grouped hits could not evade the filter by splitting into two bins. Additionally, probes were checked for matches with a BLAST[53] database constructed from common repeating sequences in mammals. The FASTA file for 'Simple Repeat' sequences for 'Mammalia only' was downloaded from Repbase[54]. All probes with at least 19 matched bases with the repeats index were dropped. After filtering the probes, all remaining probes were evaluated for potential cross-hybridization using BLAST[53]. Any probe pairs with at least 19 matched bases were dropped in the final probe selection.

Final probe sets were selected to maintain probe specificity, and to achieve a relatively uniform spacing of probes on the target sequence. Final probes were selected one by one, starting with the target region with the fewest remaining probes. The probe that minimized the sum of the squares of distances between adjacent selected probes and the start and end coordinates of the target region was selected. After selecting a probe, any probes that were found to cross-hybridize with at least 19 nt to the selected probe were dropped. As probes were added, their off-target hits were summed by bin. If the addition of a probe resulted in any bin having 10 total hits, all remaining unselected probes that had an off-target hit in that bin were dropped. For channel 1 and 2 probes, once 200 probes were selected for a target region, all remaining probes for that region were dropped. These two channels labelled 2,460 loci spaced approximately 1 Mb apart (1.04 ± 0.78 Mb as mean ± s.d.) across the whole genome. For the channel 3 probes, regions containing up to 150 probes were kept and other regions were dropped, and as a result, 1.5–2.4 Mb of 20 distinct regions containing 60 of 25-kb regions were finally selected as the 1,200 loci.

Primary probes were then assembled similar to previous seqFISH studies[18–21,55]. At each locus targeted, we used up to 200 primary probes within the 25-kb genomic region as described above to image individual loci as diffraction limited spots based on DNA FISH[56–59] and Oligopaint[16] technologies. For Mb resolution DNA seqFISH+ in channel 1 and 2, primary probes consist of the genomic region specific 35-nt sequences, flanked by the five unique 15-nt readout probe binding sequences, which correspond to pseudo-channel in each barcoding round, and a pair of 20-nt primer binding sites at the 5′ and 3′ end of the probe. For 25-kb resolution DNA seqFISH+ in channel 3, primary probes consist of the genomic region specific 35-nt sequences, flanked by three identical binding sites of a 15-nt readout probe, which corresponds to one of the 60 sequential rounds for the diffraction limited spot imaging, and two identical binding sites for a 15-nt readout probe, which corresponds to one of the 20 distinct regions for the chromosome painting, and 20-nt primer binding sites at the 5′ and 3′ end of the probes.

Primary probe synthesis

Primary probes were generated from oligoarray pools (Twist Bioscience) as previously described[18–21,55] with some modifications. In brief, probe sequences were amplified from the oligonucleotide pools with limited two-step PCR cycles (first step PCR primers, 4-fwd: 5′-ATGCGCTGCAACTGAGACCG; 4-rev: 5′-CTCGACCAAGGCTGGCACAA; second step PCR primers, 4-fwd: 5′-ATGCGCTGCAACTGAGACCG; 4-T7rev: 5′-TAATACGACTCACTATAGCTCGACCAAGGCTGGCACAA), and PCR products were purified using QIAquick PCR Purification Kit (Qiagen 28104). Then in vitro transcription (NEB E2040S) followed by reverse transcription (Thermo Fisher EP0751) were performed.

For the DNA seqFISH+ primary probes, the forward primer (4-fwd) with 5′ phosphorylation was used at the reverse transcription step to allow ligation of the primary probes as described below (see 'Cell culture experiment'). After reverse transcription, the single-stranded DNA (ssDNA) probes were alkaline hydrolysed with 1 M NaOH at 65 °C for 15 min to degrade the RNA templates, and then neutralized with 1 M acetic acid. Then, probes were ethanol precipitated, and eluted in nuclease-free water.

For the repetitive-element DNA FISH probes, LINE1 and SINEB1 probes were similarly generated except using mouse genomic DNA template extracted from E14 mouse ES cells with DNeasy Blood and Tissue Kits (Qiagen 69504) for PCR, followed by in vitro transcription and reverse transcription steps. Primers for LINE1 and SINEB1[33] contain readout probe binding sites as overhangs to allow readout probe hybridization and stripping with seqFISH routines. Genome targeting sequences of the primary probes were 113 nt and 117 nt for LINE1 and SINEB1, respectively. By contrast, the centromeric MinSat and telomere probes were generated as dye-conjugated 15-nt probes in the same way as readout probes (see 'Readout probe design and synthesis') using the following sequences (MinSat: 5′-CACTGTTCTACAATG; telomere: 5′-AACCCTAACCCTAAC), which directly target genomic DNA.

Readout probe design and synthesis

Readout probes of 12–15-nt in length were designed for seqFISH as previously described[20,21]. In brief, a set of probe sequences was randomly generated with combinations of A, T, G or C nucleotides with a GC-content range of 40–60%. To minimize cross-hybridization between the readout probes, any probes with ten or more contiguously matching sequences between the readout probes were removed. The readout probes for sequential immunofluorescence were similarly designed except the C nucleotide was omitted[60]. The 5′ amine-modified DNA oligonucleotides (Integrated DNA Technologies) with the readout probe sequences were conjugated in-house to Alexa Fluor 647–NHS ester (Invitrogen A20006) or Cy3B–NHS ester (GE Healthcare PA63101) or Alexa Fluor 488–NHS (Invitrogen A20000) as described before[20,21], or fluorophore conjugated DNA oligonucleotides were purchased from Integrated DNA Technologies. In total, 240 unique readout probes[21] were designed and synthesized for DNA seqFISH+ experiments, and subsets of those readout probes were used for RNA seqFISH experiments.

DNA–antibody conjugation

Preparation of oligonucleotide DNA conjugated primary antibodies was performed as previously described[31] with modifications. In brief, to crosslink thiol-modified oligonucleotides to lysine residues on antibodies, BSA-free antibodies were purchased from commercial vendors whenever possible. Antibodies (90–100 µg) were buffer-exchanged to 1 × PBS using 7K MWCO Zeba Spin Desalting Columns (Thermo Scientific 89882), and reacted with 10 equivalents of PEGylated SMCC cross-linker (SM(PEG)2) (Thermo Scientific 22102) diluted in anhydrous DMF (Vector Laboratories S4001005). The solution was incubated at 4 °C for 3 h, and then purified using 7K MWCO Zeba Spin Desalting Columns. In parallel, 300 µM 5′ thiol-modified 18-nt DNA oligonucleotides (Integrated DNA Technologies) were reduced by 50 mM dithiothreitol in 1× PBS at room temperature for 2 h, and purified using NAP5 columns (GE Healthcare 17-0853-01). Then maleimide activated antibodies were mixed with 6–15 equivalents of the reduced form of the thiol-modified DNA oligonucleotides in 1× PBS at 4 °C overnight. DNA-primary antibody conjugates were washed with 1× PBS 4 times and concentrated using 50-KDa Amicon Ultra Centrifugal Filters (Millipore, UFC505096). The concentration of conjugated oligonucleotide DNA and antibody with BCA Protein Assay Kit (Thermo Scientific 23225) were quantified using Nanodrop.

For the BSA containing primary antibodies, SiteClick R-PE Antibody Labelling Kit (Life Technologies S10467) was used to conjugate the antibodies with 10–20 equivalent of 5′ DBCO-modified 18-nt DNA oligonucleotides (Integrated DNA Technologies). The oligonucleotide-conjugated antibodies were validated by SDS–PAGE gel and immunofluorescence, and stored in 1× PBS at −80 °C as small aliquots.

Cell culture and preparation

E14 mouse ES cells (E14Tg2a.4) from Mutant Mouse Regional Resource Centers were maintained under serum/LIF condition as previously described[20,41]. A stable E14 line that targets endogenous repetitive regions with the CRISPR–Cas system[61] was generated similarly to the previous study[19]. In brief, PiggyBac vectors, PGK-NLS-dCas9-NLS-3xEGFP, carrying a separate puromycin resistance cassette under an EF1 promoter, and mU6-sg3632454L22Rik(F+E), carrying a separate neomycin resistance cassette under a SV40 promoter, were constructed. A single-guide RNA (sgRNA) sequence (5′-GGAAGCCAGCTGT) was used to target repetitive regions at the 3632454L22Rik gene locus in X chromosome. To create the stable E14 line (GFP/Neo E14) with those vectors, transfection was performed with FuGENE HD Transfection Reagent (Promega E2311), and cells were selected with puromycin (Gibco A1113803) at 1 µg ml^{-1}. After the selection, single clones were isolated manually, and stable labelling of the locus was verified by imaging. The cell lines were authenticated by DNA seqFISH+ (Extended Data Fig. 3a–g), multiplexed immunofluorescence (Extended Data Fig. 6a–f), and RNA seqFISH (Extended Data Fig. 9a–c), all of which gave results consistent with the ES cell identity. The cells were not tested for mycoplasma contamination.

E14 cells were plated on poly-D-lysine (Sigma P6407) and human laminin (BioLamina LN511) coated coverslips (25 mm × 60 mm)[20], and incubated for 24 or 48 h. Then cells were fixed with freshly made 4% formaldehyde (Thermo Scientific 28908) in 1× PBS (Invitrogen AM9624) at room temperature for 10 min. The fixed cells were washed with 1× PBS a few times, and stored in 70% ethanol at −20 °C[12]. In the case of co-culture experiments with unlabelled E14 cells and the GFP/Neo E14 cells (monoclonal line), cell densities were counted and cell lines were mixed with a 1:10 ratio.

Cell culture experiment

The fixed and stored cell samples were dried, and permeabilized with 0.5% Triton-X (Sigma-Aldrich 93443) in 1× PBS at room temperature for 15 min after attaching a sterilized silicon plate (McMASTER-CARR 86915K16) with a punched hole to the coverslip to use it as a chamber. The samples were washed three times with 1× PBS and blocked at room temperature for 15 min with blocking solution consisted of 1× PBS, 10 mg ml^{-1} UltraPure BSA (Invitrogen AM2616), 0.3% Triton-X, 0.1% dextran sulfate (Sigma D4911) and 0.5 mg ml^{-1} sheared Salmon Sperm DNA (Invitrogen AM9680). Then DNA oligonucleotide-conjugated primary antibodies listed below were incubated in the blocking solution with 100-fold diluted SUPERase In RNase Inhibitor (Invitrogen AM2694) at 4 °C overnight. The typical final concentration of DNA conjugated primary antibodies used were estimated as 1–5 ng µl^{-1}. The samples were washed with 1× PBS three times and incubated at room temperature for 15 min, before post-fixing with freshly made 4% formaldehyde in 1× PBS at room temperature for 5 min. Next, the samples were washed with 1× PBS six times and incubated at room temperature for 15 min. The samples were then further post-fixed with 1.5 mM BS(PEG)5 (PEGylated bis(sulfosuccinimidyl)suberate) (Thermo Scientific A35396) in 1× PBS at room temperature for 20 min, followed by quenching with 100 mM Tris-HCl pH7.4 (Alfa Aesar J62848) at room temperature for 5 min. After the post-fixation, the samples were washed with 1× PBS and air dried after removing the custom silicon chamber.

The oligonucleotide DNA-conjugated primary antibodies used were as follows: mH2A1 (Abcam ab232602), E-cadherin (R&D AF748), fibrillarin (C13C3) (Cell Signaling 2639BF), geminin (Abcam ab238988), GFP (Invitrogen G10362), H3 (Active Motif 39763), H3K27ac (Active Motif

39133), H3K27me2 (Cell Signaling 9728BF), H3K27me3 (Cell Signaling 9733BF), H3K4me1 (Cell Signaling 5326S), H3K4me2 (Cell Signaling 9725BF), H3K4me3 (Active Motif 39915), H3K9ac (Active Motif 91103), H3K9me2 (Abcam ab1220), H3K9me3 (Diagenode MAb-146-050), H3pSer10 (Millipore 05-806), H4K16ac (EMD Millipore 07-329), H4K20me1 (Abcam ab9051), H4K20me2 (Abcam ab9052), H4K20me3 (Active Motif 39671), lamin B1 (Abcam ab220797), RNAPII(Ser5P) (Abcam ab5408), SF3A66 (Abcam ab77800). Two antibodies (E-cadherin and GFP) were only included in the clonal tracing experiments. Several antibodies (H3, H3K4me1, H3K4me2 and H3K4me3) were excluded from the downstream analysis owing to the quality of antibody staining with oligonucleotide conjugation.

After the immunofluorescence preparation above, custom-made flow cells (fluidic volume about 30 µl), which were made from glass slide (25 × 75 mm) with 1-mm thickness and 1-mm diameter holes and a PET film coated on both sides with an acrylic adhesive with total thickness 0.25 mm (Grace Bio-Labs RD481902), were attached to the coverslips. The samples were rinsed with 2× SSC, and RNA seqFISH primary probe pools (1–10 nM per probe) and 10 nM polyT LNA oligonucleotide with a readout probe binding DNA sequence (Qiagen) were hybridized in 50% hybridization buffer consisted of 50% formamide (Invitrogen AM9342), 2× SSC and 10% (w/v) dextran sulfate (Millipore 3710-OP). The hybridization was performed at 37 °C for 24–72 h in a humid chamber. After hybridization, the samples were washed with a 55% wash buffer consisting of 55% formamide, 2× SSC and 0.1% Triton X-100 at room temperature for 30 min, followed by three rinses with 4× SSC. Then samples were imaged for RNA seqFISH as described below (see ‘seqFISH imaging’). Note that immunofluorescence signals were imaged at this step for validation in Extended Data Fig. 2f, g.

After RNA seqFISH imaging, the samples were processed for DNA seqFISH+ primary probe hybridization. The samples were rinsed with 1× PBS, and incubated with 100-fold diluted RNase A/T1 Mix (Thermo Fisher EN0551) in 1× PBS at 37 °C for 1 h. Then samples were rinsed three times with 1× PBS, followed by three rinses with a 50% denaturation buffer consisting of 50% formamide and 2× SSC and incubation at room temperature for 15 min. Then the samples were heated on the heat block at 90 °C for 4.5 min in the 50% denaturation buffer, by sealing the inlet and outlet of the custom chamber with aluminium sealing tapes (Thermo Scientific 232698). After heating, the samples were rinsed with 2× SSC, and DNA seqFISH+ primary hybridization buffer consisting of about 1 nM per probe, about 1 µM LINE1 probe, about 1 µM SINEB1 probe, 100 nM 3632454L22Rik fiducial marker probe (Integrated DNA Technologies), 40% formamide, 2× SSC and 10% (w/v) dextran sulfate (Millipore 3710-OP) was hybridized at 37 °C for 48–96 h in a humid chamber. After hybridization, the samples were washed with a 40% wash buffer consisting of 40% formamide, 2× SSC and 0.1% Triton X-100 at room temperature for 15 min, followed by three rinses with 4× SSC.

Then samples were further processed to ‘padlock’[62,63] primary probes to prevent the loss of signals during 80 rounds of DNA seqFISH+ imaging routines (see ‘seqFISH imaging’). A global ligation bridge oligonucleotide (Integrated DNA Technologies) was hybridized in a 20% hybridization buffer consisting of 20% formamide, dextran sulfate (Sigma D4911) and 4× SSC at 37 °C for 2 h. The 31-nt global ligation bridge (5′-TCAGTTGCAGCGCATGCTCGACCAAGGCTGG) was designed to hybridize to 15 nt of the DNA seqFISH+ primary probes at 5′ end and 16 nt at the 3′ end. Then, samples were washed with 10% WB (10% formamide, 2× SSC and 0.1% Triton X-100) three times and incubated at room temperature for 5 min. After three rinses with 1× PBS, the samples were then incubated with 20-fold diluted Quick Ligase in 1 × Quick Ligase Reaction Buffer from Quick Ligation Kit (NEB M2200) supplemented with additional 1 mM ATP (NEB P0756) at room temperature for 1 h to allow ligation reaction between 5′- and 3′-ends of the DNA seqFISH+ primary probes. Unlike the conventional padlock primary probe design[62,63], our primary probe ligation sites were on the 31-nt global ligation bridge at the primer binding sites (Extended Data Fig. 1a, b), and not on the genomic DNA. Then the samples were washed with a 12.5% wash buffer consisting of 12.5% formamide, 2× SSC and 0.1% Triton X-100, followed by three rinses with 1× PBS.

The samples were then processed for amine modification and post-fixation to further stabilize the primary probes. The samples were rinsed with 1 × labelling buffer A, followed by incubation with tenfold diluted Label IT amine modifying reagent in 1× labelling buffer A from Label IT nucleic acid modifying reagent (Mirus Bio MIR 3900) at room temperature for 45 min. After three rinses with 1× PBS, the samples were fixed with 1.5 mM BS(PEG)5 in 1× PBS at room temperature for 30 min, followed by quenching with 100 mM Tris-HCl pH7.4 at room temperature for 5 min. The samples were washed with a 55% wash buffer at room temperature for 5 min, and rinsed with 4× SSC three times. Then samples were imaged for DNA seqFISH+ and sequential immunofluorescence as described below (see ‘seqFISH imaging’).

The 1,000-gene intron experiments in Fig. 3c–e and Extended Data Fig. 8h, k were performed similarly with minor modifications. E14 coverslips were prepared and processed by following the sequential immunofluorescence steps above. After the sequential immunofluorescence preparation, 1,000-gene intron FISH probes[20] were hybridized in the 50% hybridization buffer at 37 °C for 24 h in a humid chamber. Then samples were washed with the 55% wash buffer at 37 °C for 30 min, followed by three rinses with 4× SSC. Then samples were imaged for intron FISH and sequential immunofluorescence as described below (see ‘seqFISH imaging’).

The telomere validation experiments in Extended Data Fig. 2a, b were performed similarly with minor modifications. Samples were prepared as described above and hybridized with a telomere primary probe, consisting of 20-nt telomere targeting sequence, five 15-nt readout probe binding sites and 20-nt primer binding sites with 5′ phosphorylation, in the 20% hybridization buffer at 37 °C overnight in a humidity chamber. Then samples were prepared with or without ligation and post-fixation steps as described above. After samples were imaged with the imaging procedure (see ‘seqFISH imaging’), samples were incubated in the 55% WB at 37 °C for 16 h. Then the original positions were imaged again under the same imaging procedure (see ‘seqFISH imaging’) to evaluate the padlocking efficiency across different conditions.

Microscope setup

All imaging experiments were performed with the imaging platform and fluidics delivery system similar to those previously described[20,21]. The microscope (Leica DMi8) was equipped with a confocal scanner unit (Yokogawa CSU-W1), a sCMOS camera (Andor Zyla 4.2 Plus), 63 × oil objective lens (Leica 1.40 NA), and a motorized stage (ASI MS2000). Fibre-coupled lasers (643, 561, 488 and 405 nm) from CNI and Shanghai Dream Lasers Technology and filter sets from Semrock were used. The custom-made automated sampler was used to move designated readout probes in hybridization buffer from a 2.0-ml 96-well plate through a multichannel fluidic valve (IDEX Health & Science EZ1213-820-4) to the custom-made flow cell using a syringe pump (Hamilton Company 63133-01). Other buffers were also moved through the multichannel fluidic valve to the custom-made flow cell using the syringe pump. The integration of imaging and the automated fluidics delivery system was controlled by custom-written scripts in µManager[64].

seqFISH imaging

The sequential hybridization and imaging routines were performed similarly to those previously described[20,21] with some modifications. In brief, the sample with the custom-made flow cell was first connected to the automated fluidics system on the motorized stage on the microscope. Then the regions of interest (ROIs) were registered using nuclei signals stained with 5 µg ml^{-1} DAPI (Sigma D8417) in 4× SSC. RNA seqFISH imaging was performed with the sequential hybridization and imaging routines described below first. After the completion of RNA seqFISH imaging, the samples were disconnected from the microscope, and proceeded to the DNA seqFISH+ procedures (see ‘Cell culture experiment’). For the DNA seqFISH+ and sequential immunofluorescence imaging, the registered ROIs for RNA seqFISH were loaded and manually corrected to ensure to image the same ROIs as RNA seqFISH imaging, and following routines were performed.

All the sequential hybridization and imaging routines below were performed at room temperature. The serial hybridization buffer contained two or three unique readout probes (10–50 nM) with different fluorophores (Alexa Fluor 647, Cy3B or Alexa Fluor 488) in 10% EC buffer (10% ethylene carbonate (Sigma E26258), 10% dextran sulfate (Sigma D4911) and 4× SSC), and was picked up from a 96-well plate and flow into the flow cell for 20 min incubation. For DNA seqFISH+ experiments, readout probes (Alexa Fluor 647, Cy3B or Alexa Fluor 488) for sequences designated as fiducial markers were also included in the serial hybridization buffer to allow image registration at the subpixel resolution. After the serial hybridization, the samples were washed with 1 ml of 4× SSCT (4× SSC and 0.1% Triton-X), followed by a wash with 330 μl of the 12.5% wash buffer. Then, the samples were rinsed with about 200 μl of 4× SSC, and stained with about 200 μl of the DAPI solution for 30 s. Next, anti-bleaching buffer was flown through the sample for imaging. The anti-bleaching buffer was made of 50 mM Tris-HCl pH 8.0 (Invitrogen 15568025), 300 mM NaCl (Invitrogen AM9759), 2× SSC, 3 mM trolox (Sigma 238813), 0.8% D-glucose (Sigma G7528), 1,000-fold diluted catalase (Sigma C3155), 0.5 mg ml^{-1} glucose oxidase (Sigma G2133)[20] for E14 experiments, and made of 50 mM Tris-HCl pH 8.0, 4× SSC, 3 mM trolox, 10% D-glucose, 100-fold diluted catalase, 1 mg ml^{-1} glucose oxidase (Sigma G2133)[21] for unlabelled E14 and GFP/Neo E14 line clonal experiments.

Snapshots were acquired with 0.25-μm *z*-steps over 6-μm *z*-slices with 643-nm, 561-nm, 488-nm and 405-nm fluorescent channels per field of view, except for RNA seqFISH in the clonal experiments, which were acquired with 0.75-μm *z*-steps with 643-nm, 561-nm and 488-nm fluorescent channels. After image acquisition, 1 ml of the 55% wash buffer was flown for 1 min to strip off readout probes, followed by an incubation for 1 min before rinsing with 4× SSC. The serial hybridization, imaging and signal extinguishing steps were repeated until the completion of all rounds. During the RNA seqFISH and DNA seqFISH+ imaging routines, blank images containing only autofluorescence of the cells were imaged at the beginning and end of the routines. During the DNA seqFISH+ imaging, images containing only fiducial markers were also imaged at the beginning and at the end of the routines for the image alignment (see ‘Image analysis’). Images were manually checked at the end of all imaging routines and in case problematic hybridization rounds such as off-focus appeared, those hybridization rounds were repeated.

Each readout probe hybridization and stripping routine took approximately 30 min. Imaging time per position took around 2.5–6 min at each hybridization round with our microscope setup and imaging conditions described above, and we typically imaged for 30 min per hybridization round with 5–10 positions. In total, it took approximately 80 h to complete the 80 rounds of the hybridization and imaging routine for the DNA seqFISH+ experiments.

Image analysis

To correct for the non-uniform background, a flat field correction was applied by dividing the normalized background illumination with each of the fluorescence images while preserving the intensity profile of the fluorescent points. The background signal was then subtracted using the ImageJ rolling ball background subtraction algorithm with a radius of 3 pixels.

FISH spot locations were obtained by using a Laplacian of Gaussians filter, semi-manual thresholding as described below, and a 3D local maxima finder. Subsequently the locations were super resolved using a 3D radial centre algorithm[65,66]. In brief, a 3 × 3 × 3 cube of pixels around a local maxima found above the specified threshold was taken from the aligned and background subtracted image. This sub-image was then used to calculate the sub-pixel location of the RNA molecule or DNA locus and the mean standard deviation (average of the standard deviation in each dimension) of the intensity cloud using a 3D radial centre algorithm. A MATLAB implementation of the algorithm can be found on the Parthasarathy lab website (https://pages.uoregon.edu/raghu/particle_tracking.html). The resulting RNA or DNA spot locations were further filtered on the basis of the size of the sigma values.

To find the optimal threshold values for the spot detection, threshold values for RNA seqFISH were updated manually. By contrast, for DNA seqFISH+, 29 incremental threshold values, were initially applied to the images in the first position. The number of spots and median spot intensity in the nuclei were computed for each of the 29 thresholds across 80 hybridizations. Then the threshold value for the first hybridization round was manually chosen, and threshold for the other hybridizations were selected such that the number of dots detected matches most closely to those expected from the codebook. For example, if hyb1 targets 30 loci and hyb2 targets 60 loci, then hyb2 should have twice as many dots as hyb1. In this process, we assumed all loci can be detected with the same detection efficiency on average. In addition, the median intensities from the adjacent threshold values were compared, and whenever intensity differences were more than 15%, a more stringent threshold value was taken to fulfill this criteria to minimize non-specific spot detection. These processes were performed in individual fluorescent channels independently. Similarly, we corrected the threshold values across positions by computing the ratio of the median intensities relative to those from the first position per hybridization in order to minimize detection bias across different positions.

To align spots or images in different channels to those in the reference channel (643 nm), chromatic aberration shifts were corrected using the fiducial markers to calculate the offsets. To align RNA seqFISH and sequential immunofluorescence images in different hybridization rounds, reference channels (either DAPI or polyA staining) were aligned using 2D phase correlations along every axis iteratively to find a consensus transformation for alignment as previously described[20]. The 2D phase correlation algorithm is implemented in MATLAB with the function imregcorr. To align DNA seqFISH+ spots in different hybridization rounds, fiducial markers were identified in each image by searching for the known ‘constellation’ seen in images containing only the fiducial markers. To identify a first pair of distant fiducial markers, the vector describing the relative position of the known markers was compared with those separating similarly oriented pairs of FISH spots in each image. Most, if not all, of the fiducial marker ‘constellation’ can then be recovered by searching for each fiducial marker at its known location relative to that of previously identified fiducial markers in the image. Further alignment to correct any rotation between RNA and DNA FISH images was done as follows. First, both image stacks to be aligned (DAPI or immunostaining) were converted to 2D images using a maximum intensity projection in the *z*-dimension. The resulting 2D images were aligned using a one plus one evolutionary optimization method to maximize the Mattes mutual information between the images with the transformation constrained to only rigid transforms with a maximum of 500 iterations. This algorithm is implemented in MATLAB with the function imregtform. Once 2D alignment with both translation and rotation was obtained, one stack was transformed using the found transformation. The image stacks were then projected along the *x* axis and aligned using a normalized cross-correlation to determine the first estimate of the *z*-dimension offset. The image was then projected along the *y* axis to find a second estimate of the *z*-dimension offset using the same method. The two offsets were averaged.

To assign mRNA spots to individual cells, the processed spots were collected within individual cytoplasmic ROIs, which were segmented manually from polyA or E-cadherin images. Similarly, to assign intron and DNA spots to individual cells, the spots within individual nuclear ROIs from DAPI images[20] were collected. By comparing the centroids between cytoplasmic ROIs and nuclear ROIs, numbers from both ROIs were matched. Only cells at the centre of the fields of view were preserved for the RNA analysis to avoid biasing the RNA distribution.

For channel 1 and 2 barcode decoding in DNA seqFISH+, once all potential points in all hybridizations were obtained, points were matched to potential barcode partners in all other barcoding rounds of all other hybridizations using a 1.73 (square root of 3) pixel search radius to find symmetric nearest neighbours in 3D. This process was performed in each nuclear ROIs. Point combinations that constructed only a single barcode were immediately matched to the on-target barcode set. Two rounds of error correction were implemented out of five total barcoding rounds. For points that matched to multiple barcodes, the point sets were filtered by calculating the residual spatial distance of each potential barcode point set and only the point sets giving the minimum residuals were used to match to a barcode. If multiple barcodes were still possible, the point was matched to its closest on-target barcode with a hamming distance of 1. If multiple on target barcodes were still possible, then the point was dropped from the analysis as an ambiguous barcode. This procedure was repeated using each barcoding round as a seed for barcode finding and only barcodes that were called similarly in at least 4 out of 5 seeds were used in the analysis. This criteria on average dropped 19.8 ± 2.8% (mean ± standard deviation) of identified barcode spots compared to the less stringent criteria using at least 3 out of 5 seeds, while minimizing the detection of false positive barcode dots. The false negatives can be caused by this dropout of barcode dots as well as by incomplete denaturation of chromosomal DNA or hybridization of primary probes. For the false positive estimates, both blank barcodes and on-target barcodes were run simultaneously. Those blank barcodes consisted of all the remaining barcodes out of 2,048 barcodes that allow 2 rounds of error correction in 5 total barcoding rounds.

For channel 3 decoding in DNA seqFISH+, once all potential points in the first 60 hybridizations (hyb1–60) were obtained, intensities of all the potential chromosome paint partners in the other 20 hybridizations (hyb61–80) were computed on the rounded pixels where points were found. At this step, each point has 20 intensity values, corresponding to those from individual chromosome paints. Those chromosome paint intensities found on the points in nuclei from all positions and all hybridization rounds (hyb1–60) were grouped by chromosome, and then z score was calculated. The *z*-score values were thresholded with 1, and each point was assigned with unique chromosome identity, whose value was above the threshold. Only a minimum fraction of points (<3%) were assigned to multiple chromosomes and dropped as ambiguous points. In addition, points without any chromosome assignment were dropped as ambiguous points.

Exterior and interior voxels of immunofluorescence markers

For the sequential immunofluorescence image processing, in contrast to spot detection processing as described above, background subtraction was not applied to the images, except for marker edge detection described below and RNAP II Ser5-P visualization shown in Fig. 3d and Extended Data Fig. 8h. The alignment and correction for chromatic aberration shifts between different fluorescent channels were performed as described above. Then intensity values for all the voxels within individual nuclear ROIs were obtained for all immunofluorescence channels as well as repetitive elements (telomere, MinSat, LINE1 and SINEB1) and DAPI. The edge detection for chromatin marker exterior quantification was performed using the Find edges function in ImageJ with background subtracted images (rolling ball radius 3 pixels), and then the intensity values were obtained in the same way as the aligned images above.

After image processing steps above, pixel information was converted to physical distance based on the microscope setup and imaging condition with 103 nm for *x* and *y* pixels and 250 nm for *z* pixels for the subsequent downstream analysis.

Analysis of sequencing-based data

Hi-C data from NCBI GEO (accession GSE96107) was processed using Juicer tools[67] and contact maps containing Knight–Ruiz normalized counts[68] were obtained. SPRITE data were obtained from the 4D Nucleome data portal (https://data.4dnucleome.org/, accession 4DNESOJRTZZR). ChIP–seq data for H3K27me3, H3K9ac and H3K27ac were obtained from ENCODE (https://www.encodeproject.org/, accession ENCSR000CFN, ENCSR000CGP and ENCSR000CGQ) as bigWig tracks and the average relative signal in each genomic bin was calculated using the UCSC Genome Browser program bigWigAverageOverBed. DamID data were obtained from NCBI Gene Expression Omnibus (GEO) (accession GSE17051) and the genomic coordinates of DamID microarray probes were converted from mm9 to mm10 using the UCSC Genome Browser program liftover. DamID values were calculated as the mean DamID score within each genomic bin. Repli-seq data were obtained from NCBI GEO (accession GSE102076) and the replication timing at each genomic bin was calculated as the $\log_2$-transformed ratio of early and late S fractions. GRO-seq data were obtained from NCBI GEO (GSE48895) and aligned to mm10 using Bowtie2[52] to create .bam files. Read counts at each genomic bin were obtained from .bam files using bedtools multicov. Hi-C data were binned at 25-, 50-, 100-, 250-, 500-kb and 1-Mb resolution, and all the other data were binned at 1-Mb resolution. For Hi-C analysis, overlapping regions within a given bin size were excluded from the analysis (Fig. 1f with 100-kb bin resolution, Fig. 1g with 25-kb bin resolution, and Extended Data Fig. 3 with described bin resolution).

Visualization of seqFISH data

DNA seqFISH+ data were visualized using PyMOL (Molecular Graphics System, v.2.0 Schrödinger) by generating a .xyz file containing the *x*, *y* and *z* coordinates of each FISH probe coordinate. Each coordinate was displayed as a sphere, and sticks were drawn between coordinates that were consecutive in the genome. Immunofluorescence and repetitive element DNA FISH signals were visualized by displaying a surface around *x*, *y* and *z* coordinates with intensity *Z*-score values above 2.

Estimation for DNA seqFISH+ detection efficiency

We estimated the detection efficiency of DNA seqFISH+ considering the cell cycle distribution as previously described[19]. In brief, typical cell cycle phases distribute as 20% in G1, 50% in S and 30% in G2/M phase in mouse ES cells. Given the number of DNA loci is 2 in G1, 3 in S and 4 in G2/M phase, the average number of spots expected for each locus is 3.1 in a single cell, which can be half for chromosome X ($n = 180$ loci in DNA seqFISH+) in male diploid E14 cells. In our DNA seqFISH+ experiments, we observed 5,616.5 ± 1,551.4 (median ± s.d.) for 3,660 loci in single cells, and the detection efficiency can be estimated as 50.7 ± 14.0% (median ± s.d.).

DNA proximity map analysis

To generate a pairwise proximity map from the DNA seqFISH+ dataset, for each locus in a single cell, the identities of other loci within a search radius of 500 nm for channel 1 and 2 and 150 nm for channel 3 were tabulated. The total occurrence of any pairwise interaction was normalized by the product of the occurrence frequency of each of the loci. The proximity map was compared with the Hi-C map[23] in Fig. 1g. The proximity maps for all chromosomes for both 1-Mb and 25-kb data are shown in Extended Data Figs. 3, 4.

Physical distance versus genomic distance

In each cell, two homologous chromosomes were separated by finding the consensus between two clustering algorithms: Spectral method in the FindClusters function in Mathematica and Ward method. For most chromosomes in single cells, the two copies of homologous chromosomes occupied distinct regions in the nucleus, whereas in some cells, they were fused together. In a small percentage of cells, three or more alleles of the same chromosome could be observed. However, in a vast majority of cells, only two chromosomal territories were observed, indicating that replicated chromosomes mostly stay together[69] until segregation. For the 25-kb data, the alleles were separated by the DBSCAN clustering algorithm in scikit-learn library in Python.

Along each allele of a given chromosome in single cells, we calculated the physical distances between all pairs of detected loci and paired them with their genomic distances. For a fixed genomic distance, the median physical separation values are shown in Fig. 1h for the 1-Mb data for all the chromosomes, and Fig. 1i for the 25-kb resolution data.

Immunofluorescence normalization and clustering analysis

For the voxel-based multiplexed immunofluorescence analysis, we first aligned the sequential immunofluorescence data across all rounds of hybridization (see 'Image analysis'). Then voxels in each channel were binned 2 × 2 × 1 (200 nm × 200 nm × 250 nm), because the diffraction limit is approximately 200–250 nm in the fluorescence channels imaged. All subsequent data analyses were performed on the binned data. Because tens of millions of voxels from all of the cells were too numerous for clustering analysis, representative subsets of voxels were selected, clustered and used as a training set to train a model which then propagated the cluster identification to all voxels in the data. To do so, voxels from a single *Z*-plane (plane 13, approximately at the midpoint in the cell) out of 25 *z*-slices for all cells were selected. In each cell, individual channels were *z*-score normalized. The voxels with total *z*-score values more than 0 summed over 16 immunofluorescence channels were selected and normalized by the total *z*-score to account for voxel-to-voxel intensity variations. All pixels of the cells within the first experiment ($n = 201$ cells) were then combined and one out of every 200 pixels are selected and clustered by hierarchical clustering using the Mathematica Agglomerate function and Ward distance option. 10 clusters or nuclear zones were assigned to all 60,482 pixels as the training set. These classified zone definitions were then propagated to the rest of the pixels in each cell normalized by the above procedure using the GradientBoostedTree option in the Classify function in Mathematica. Separately, pixels with lamin B1 and fibrillarin marker *z*-score >1 were assigned to the nuclear lamina and nucleolus zones. The 44,000 pixels, which are assigned to one of the 12 nuclear zones and contain 16 intensity values from individual immunofluorescence markers, were then visualized in Extended Data Fig. 8b with uniform manifold approximation and projection (UMAP)[70] using a UMAP-learn library in Python.

To compare the immunofluorescence zone assignments with and without DNA FISH, we used the immunofluorescence data from the intron experiments. We used the same training set from the DNA seqFISH+ dataset and propagated the classifiers to the immunofluorescence data in the intron experiment. We found similar composition of zones in the intron experiments, indicating that immunofluorescence data are not affected significantly with the denaturing conditions in DNA FISH. Results are shown in Extended Data Fig. 8d.

Similarly, we downsampled the number of immunofluorescence marks used to assign the zones. We reduced the number of immunofluorescence marks systematically and used 80% of the pixels as the new training set to determine what fraction of the pixels are assigned correctly. Results are shown in Extended Data Fig. 8e. Twenty random subsets of immunofluorescence marks are drawn for each downsample immunofluorescence number. Band shows the standard deviation of the correct zone assignment.

The zone assignments are based on the combinatorial chromatin marks at each diffraction-limited pixel. Thus, the resolution and the boundary of the zones are also diffraction limited, which could contribute to some of the mixed zones detected. For example, we cautiously note that previous super-resolution imaging[71] showed that lamin B1 meshwork is around 100-nm thick at the nuclear periphery, while our zone analysis showed lamin B1 enriched zone 11 and mixed zone 12 were typically found at the pixels further than 100 nm from the nuclear periphery (Fig. 3b, Extended Data Fig. 8f–h), possibly owing to the limitation of the resolution. In addition, background signals of the multiplexed immunofluorescence could also affect the nuclear zone distribution patterns. Future works with super-resolution microscopy may resolve the mixed regions at finer resolution.

DNA loci to immunofluorescence marker interactions

We calculated the spatial distances between each DNA locus and the nearest 'hot' immunofluorescence voxel, defined as 2 s.d. above the mean value for each immunofluorescence marker. We also calculated the distance of each DNA loci to the exterior of immunofluorescence nuclear bodies, also 2 s.d. above the mean for the edge processed image described under 'Image analysis' (Extended Data Fig. 5b) for each immunofluorescence marker. Both metrics, defined as interior and exterior distances, are highly correlated (Extended Data Fig. 5e, f). From this distance metric, we generated a chromatin profile by counting the percentage of cells in which each DNA loci is within 300 nm of the surface of an immunofluorescence mark, the resolution of the diffraction-limited immunofluorescence images. These chromatin profiles were correlated with ChIP–seq[24], DamID[35], and SPRITE[7] datasets (Extended Data Fig. 6a, b).

For lamin B1, we calculated the distances from DNA loci to lamin B1 signals with two and three s.d. away from the mean intensity, as well as using only lamin B1 signals at the nuclear periphery (as determined from the convex hull of the nuclear pixels) and the nuclear periphery pixels. Similar lamin B1 or nuclear periphery association profiles were observed for all analysis in correlation plots (Extended Data Fig. 6c) across DNA loci (Extended Data Fig. 6e).

Fixed loci were determined as loci that appear 2 s.d. above the mean percentage score for each immunofluorescence mark. The distance between fixed loci and the exterior and interior of nuclear bodies, pixels 2 s.d. above the mean in the edge processed and raw images for each immunofluorescence mark, are shown in Fig. 2e. The average expression level for fixed loci associated with different immunofluorescence marks are calculated from bulk RNA-seq and shown in Extended Data Fig. 8m.

Chromosome configuration (Supplementary Table 3) of the fixed points calculates the fraction of cells ($n = 446$ cells) for each chromosome that contains at least one fixed locus from a given pair of the immunofluorescence markers. This metric measures how likely fixed points from different immunofluorescence markers are to span nuclear bodies in single cells.

Previous literature reported the approximate locations of rDNA on a subset of chromosomes with non-sequencing methods. In mouse, rDNA arrays are encoded on the centromere-proximal regions of chromosomes 12, 15, 16, 18 and 19, and the patterns of distribution differ in a mouse strain-specific manner[72–74]. We found all fixed loci for the nucleolar marker fibrillarin in those chromosomes ($n = 39$, 1, 22, 30 and 41 loci for chromosome 12, 15, 16, 18 and 19), with less enrichment on chromosome 15 (Fig. 2d, h). Previous studies using the allele of the 129 mouse strain reported the loss of rDNA or nucleolar enrichments on chromosome 15[7,73,74], consistent with our observation with E14 cells derived from the 129/Ola mouse strain.

The chromatin profiles for all loci were clustered by hierarchical clustering using the Agglomerate function in Mathematica with the Ward distance option and plotted as *t*-distributed stochastic neighbor embedding (*t*-SNE) plots (Extended Data Fig. 7a) with the scikit-learn library in Python. Fifteen chromatin marks and DAPI were used, and 4 clusters were selected. Cluster 1 was enriched in repressive markers such as H3K9me3, mH2A1 and DAPI. Cluster 2 was enriched in interactions with fibrillarin and associated with nucleolus. Cluster 3 was enriched in active marks such as RNAPII(Ser5P), H3k27ac and SF3A66 (speckle marker). Cluster 4 was enriched in lamin B1. In individual cells, loci associated with each cluster were mapped onto the chromosome structure images shown in Extended Data Fig. 7b. To calculate the spatial proximity spatial proximity of loci within and between clusters, we computed the frequency of finding a locus from a given cluster within a 1 µm radius with another locus of the same or different cluster identity. The total number of intra-cluster and inter-cluster interactions were tabulated and normalized to unity. Randomized data was generated by scrambling the cluster identities of individual loci in cells while keeping the total number of loci within each cluster the same within that cell. The proximity frequency for observed and randomized data for each cell are shown as box plots in Extended Data Fig. 7d and for different search radii in Extended Data Fig. 7e. Similar analysis is performed for A/B compartment assignments[23], and shown in Extended Data Fig. 7f–j. The loci without A/B compartment assignments in the study were excluded from the analysis.

Association of loci with zones

For each DNA locus decoded from the DNA seqFISH+ experiment, the nearest pixels within 300 nm and the zone assignments for those pixels were collected in each cell. It is possible to have a locus be in association with multiple zones. If a locus interacts with more than two zones—for example, *Pou5f1* in cell 38 interacts with zone 1, 2 and 8—then its zone interactions were divided into pairs of zones, or interfaces. In other words, that locus was counted 1/3 towards each of the interfaces (1, 2), (2, 8) and (1, 8). For individual loci, the frequencies of appearing in all zones and interfaces were normalized to unity and shown in Extended Data Fig. 8i, j. For the analysis shown in Fig. 3c and Extended Data Fig. 8k, the total number of DNA loci detected each zone and interfaces were tabulated and normalized to unity for each zone or interfaces between pairs of zones. The same analysis for zone proximity was performed on the set of loci that are interacting with other loci on the same chromosomes (intra-chromosomal) and with loci on the other chromosomes (inter-chromosomal) within 300 nm. Similarly, the introns from the 1,000-gene experiments were tabulated for their zone and interface assignments. Randomized DNA loci were generated by selecting a random set of voxels in the nucleus while keeping the total number of DNA loci the same in a given cell. Then the voxels were offset by a random *xyz* value with a 100-nm radius. To bootstrap all of the datasets, we randomly sampled 150 cells out of $n = 201$ cells with 20 trials and calculated the mean and s.e.m.

Correlation of zone with gene expression

To calculate the correlation between expression and zone assignment, we took each channel 1 and 2 locus and computed the total RNA-seq FPKM values[49] within 50 kb upstream and downstream of that locus. We normalized the total frequency of appearing in one of the zones or interfaces to unity for each loci. We then correlated the log(1 + expression value) of all 2,460 regions with the frequency of finding them in each of the zones or interfaces. Similar analysis was performed for GRO-seq[75] using log(1 + GRO-seq value) and replication timing[76] datasets with mouse ES cells.

To determine whether we can predict the mean expression values for each locus based on its zone association profiles, we estimated the expression level for a given locus as a sum of the product between the normalized frequency of being in each zone or interface for that locus and the PCC between the zone or interface with the mean expression value across all the loci. The estimated expression values for all 2,460 loci were correlated with the actual expression values with a PCC of 0.54.

For calculating the correlation between mRNA expression levels with zone assignments in single cells, we first *z*-scored the single cell mRNA seqFISH measurements for 22 genes after normalizing by *Eef2* expression levels to account for cell size differences and selecting cells in the centre field of view ($n = 125$ in replicate 1). Genes with mean copy numbers of >10 per cell were used. Lack of correlation was observed with both biological replicates, but only the cells in replicate 1 were shown to eliminate potential contributions from batch to batch variations. We counted the frequency of each of the measured loci within 300 nm of a voxel with an active or speckle zone assignment (zone 1 and 2), normalized by the total number of voxels that were within 300 nm of the DNA locus. The PCC was computed between the *z*-scored expression value and the active/speckle zone association frequency. To randomize the sample, we shuffled the *z*-score normalized expression values with active or speckle zone occupancy from different cells over 20 randomized trials. The correlation coefficient for each gene was calculated and plotted in Fig. 3i and Extended Data Fig. 8n.

To calculate the correlation between intron expression levels with zone assignments in single cells, we classified the corresponding DNA loci as 'on' or 'off' based on whether introns were bursting at that loci or not for 13 introns measured. The genes with mean burst frequencies of >0.1 per cell were used. Then the active and speckle zone occupancy for loci in each category was calculated and shown in Fig. 3j and Extended Data Fig. 8o with each point representing one intron.

Colony analysis

For cells within the unlabelled E14 colonies, we compute the correlation of the immunofluorescence states, RNA states and chromosome structures between pairs of cells. Individual RNA levels were normalized by *Eef2* expression level and then *z*-scored across all cells in the experiment. The chromosome proximity correlations between cells were computed as follows. First, a 20 × 20 chromosome to chromosome proximity matrix was generated for each cell with a search radius of 2.5 µm. Then the correlations between cells were computed as the PCC of the entries of the two matrices. The intensity of individual immunofluorescence marks was first normalized by the total intensity of all immunofluorescence marks and then *z*-scored within each field of view. The averages of the cell pair correlation values for immunofluorescence, RNA and chromosomes are shown in Fig. 4e for 24 h and 48 h clonal tracing as well as controls (correlation of pairs of cells between colonies in the 24 h and 48 h data). In addition, we computed the variance of individual immunofluorescence marks within single colonies in the 48 h experiment compared to the variance between cells of different colonies. Immunofluorescence marks that have longer time scale correlation showed lower variance within colonies compared to the variance between colonies in Fig. 4f.

Normalization of global chromatin levels in single cells

To remove the contributions from cell size, background signals, the affinity of antibody used, as well as differences between biological replicates, we constructed a generalized linear model (GLM) for the sequential immunofluorescence data using the glm() function in R, which had been used to adjust for systematic bias in single cell RNA sequencing data[77–79], for each chromatin mark *i*, using a Gaussian error distribution:

$$\log Y_i \approx \beta_0 + \sum_j \beta_j X_j$$

in which Y_i represents the vector of total fluorescence intensity of chromatin mark *i* across all cells, and X_j is a vector of latent variables contributing to the systematic bias in global chromatin states quantification. We included cell size, total fluorescence intensity over all chromatin marks per cell, experimental replicate ID and field of view (FOV) ID as latent variables in the GLM, and used the Pearson residuals of each fitting as the corrected standardized values of single cell chromatin state.

Characterizing the heterogeneity of global chromatin states in single cells

We next described the global chromatin heterogeneity between single cells using the adjusted total fluorescence intensities derived from above. Our single-cell global chromatin data has less profiled features, and without the sparsity commonly seen in many of the single cell RNA-seq datasets, we were able to directly calculate pairwise similarity of single cells from the adjusted data matrix. A k-nearest neighbour (kNN) graph was computed from the cell–cell Euclidean distance with $k = 10$ without the four cell cycle markers (geminin, H4K20me1, H3pSer10 and H4K16ac). The kNN graph was used as the input for UMAP[70] for 2D visualization (Extended Data Fig. 9d), and was also subsequently transformed into a shared nearest neighbour (SNN) graph for Leiden clustering[80], with the resolution parameter set to 0.8. The Seurat[81] functions FindNeighbours() and FindClusters() were used.

We then included four markers of cell cycle processes in the analysis: geminin, H4K20me1, H3pSer10 and H4K16ac[20,82]. We constructed a principal curve[83] which worked as a nonlinear summary of multi-dimensional data, using the function principal_curve() from the R package princurve. Using the projected values onto the principal curve as ordered cell cycle states, we found that H4K20me1 and H4K16ac displayed opposite continuum across single cells (Extended Data Fig. 9f), suggesting that the principal curve depicted a progression from G2/M to S phase.

Characterizing transcriptional heterogeneity of single cells

Similar to global chromatin states quantification, we constructed a GLM for individual gene expression vector in RNA data, with cell size, total profiled transcripts per cell, experimental replicate ID and FOV ID as latent variables. Pearson residuals were taken as the corrected and standardized expression values.

Given that the majority of mRNA species in this dataset are pluripotency and differentiation genes (for example, *Nanog*, *Pou5f1* and *Dnmt3a*), we were interested in whether cells could be ordered pseudo-temporally in transcriptional states. We used a diffusion map[84,85] to infer a low-dimensional manifold of RNA seqFISH data with the package destiny[86], and the first diffusion component in rank was taken as a measurement of pseudotime. All the profiled genes were used to construct pseudotime, except for *Cx3cr1*, *Npy*, *S100b* and *Zfp352* (maximum transcript count less than 10 in a cell). To visualize the continuum transcriptional and global chromatin data with respect to pseudotime progression, for every transcript and chromatin mark, we performed a local polynomial regression fitting with span = 0.75 and degree = 2 and generated the fitted values (Extended Data Fig. 9h).

Mapping RNA seqFISH data to scRNA-seq results

To evaluate whether transcriptional states of mouse ES cells from seqFISH were comparable to those measured by single cell RNA-seq, we constructed a support vector machine (svm) model for mapping seqFISH data to existing scRNA-seq results. Specifically, scRNA-seq data[42] was downloaded from ArrayExpress, and we retrieved quantifications for cells cultured in serum/LIF condition for analysis. The top 2,000 most variable genes were identified based on dispersion, based on which we ran a principal component analysis (PCA) and used the top 30 components as input for Leiden clustering[80], with the resolution parameter set to 0.8 in the Seurat[81] function FindClusters(). For data alignment between mouse ES cells quantified by the two technologies, we performed canonical correlation analysis (CCA) to project the two datasets onto a shared space, followed by L2 normalization, using genes detected by both scRNA-seq and seqFISH (40 mRNA markers in total). The aligned data was for svm training and prediction, where the classifier was trained on cells captured by scRNA-seq with tenfold cross validation, and cluster labels were subsequently transferred to aligned seqFISH data. For joint visualization, we performed UMAP on the L2-normalized CCA embeddings for all cells (Extended Data Fig. 9b).

Statistics and reproducibility

Cells shown in Figs. 1b–d, 2a, 4a, Extended Data Figs. 4a, 5a, b are representative of the 446 cells imaged in 2 biological replicates. Cells shown in Fig. 3 are representative of 201 cells and 172 cells in two independent experiments. Cells shown in Fig. 4d and Extended Data Fig. 10a are representative of $n = 117$ cells in the 48-h dataset.

Network analysis

To investigate the relationship of gene and chromatin markers, we first calculated the pairwise PCC of different genes and chromatin markers using a scaled mRNA/antibody × cell matrix (Extended Data Fig. 9e). Then, the results were represented as a network, where a gene–gene, chromatin mark–chromain mark or gene–chromatin mark pair were connected if the PCC was greater than 0.4. The network was visualized using Cytoscape[87], and the widths of edges in network were weighted by $100^{|PCC|}$ to highlight the edges with high correlation (Extended Data Fig. 9i).

Reporting summary

Further information on research design is available in the Nature Research Reporting Summary linked to this paper.

Data availability

The source data and processed data from this study are available at Zenodo (https://zenodo.org/record/3735329). Additional raw microscopy data obtained during this study are available from the corresponding author upon reasonable request. Publicly available datasets used in the study (GSE96107, 4DNESOJRTZZR, GSE17051, GSE102076, GSE48895, ENCSR000CFN, ENCSR000CGP, ENCSR000CGQ) are detailed in the Methods.

Code availability

The custom written scripts used in this study are available at https://github.com/CaiGroup/dna-seqfish-plus.

50. Cunningham, F. et al. Ensembl 2019. *Nucleic Acids Res*. **47**, D745–D751 (2019).
51. Klein, A. M. et al. Droplet barcoding for single-cell transcriptomics applied to embryonic stem cells. *Cell* **161**, 1187–1201 (2015).
52. Langmead, B. & Salzberg, S. L. Fast gapped-read alignment with Bowtie 2. *Nat. Methods* **9**, 357–359 (2012).
53. Camacho, C. et al. BLAST+: architecture and applications. *BMC Bioinformatics* **10**, 421 (2009).
54. Bao, W., Kojima, K. K. & Kohany, O. Repbase Update, a database of repetitive elements in eukaryotic genomes. *Mob. DNA* **6**, 11 (2015).
55. Eng, C. L., Shah, S., Thomassie, J. & Cai, L. Profiling the transcriptome with RNA SPOTs. *Nat. Methods* **14**, 1153–1155 (2017).
56. Cremer, C. et al. in *Handbook of Computer Vision and Applications* Vol. 3 (ed. Jahne, B. et al) 839–857 (Academic, 1999).
57. Croft, J. A. et al. Differences in the localization and morphology of chromosomes in the human nucleus. *J. Cell Biol*. **145**, 1119–1131 (1999).
58. Esa, A. et al. Three-dimensional spectral precision distance microscopy of chromatin nanostructures after triple-colour DNA labelling: a study of the BCR region on chromosome 22 and the Philadelphia chromosome. *J. Microsc*. **199**, 96–105 (2000).
59. Cremer, M. et al. Multicolor 3D fluorescence in situ hybridization for imaging interphase chromosomes. *Methods Mol. Biol*. **463**, 205–239 (2008).
60. Zhang, Z., Revyakin, A., Grimm, J. B., Lavis, L. D. & Tjian, R. Single-molecule tracking of the transcription cycle by sub-second RNA detection. *eLife* **3**, e01775 (2014).
61. Chen, B. et al. Dynamic imaging of genomic loci in living human cells by an optimized CRISPR/Cas system. *Cell* **155**, 1479–1491 (2013).
62. Nilsson, M. et al. Padlock probes: circularizing oligonucleotides for localized DNA detection. *Science* **265**, 2085–2088 (1994).
63. Rouhanifard, S. H. et al. ClampFISH detects individual nucleic acid molecules using click chemistry-based amplification. *Nat. Biotechnol*. (2018). https://doi.org/10.1038/nbt.4286
64. Edelstein, A., Amodaj, N., Hoover, K., Vale, R. & Stuurman, N. Computer control of microscopes using µManager. *Curr. Protoc. Mol. Biol*. **Ch. 14**, Unit14.20 (2010).
65. Liu, S.-L. et al. Fast and high-accuracy localization for three-dimensional single-particle tracking. *Sci. Rep*. **3**, 2462 (2013).
66. Parthasarathy, R. Rapid, accurate particle tracking by calculation of radial symmetry centers. *Nat. Methods* **9**, 724–726 (2012).
67. Durand, N. C. et al. Juicer provides a one-click system for analyzing loop-resolution Hi-C experiments. *Cell Syst*. **3**, 95–98 (2016).
68. Knight, P. A. & Ruiz, D. A fast algorithm for matrix balancing. *IMA J. Numer. Anal*. **33**, 1029–1047 (2013).
69. Stanyte, R. et al. Dynamics of sister chromatid resolution during cell cycle progression. *J. Cell Biol*. **217**, 1985–2004 (2018).
70. McInnes, L., Healy, J., Saul, N. & Großberger, L. UMAP: uniform manifold approximation and projection. *J. Open Source Softw*. **3**, 861 (2018).

71. Nmezi, B. et al. Concentric organization of A- and B-type lamins predicts their distinct roles in the spatial organization and stability of the nuclear lamina. *Proc. Natl Acad. Sci. USA* **116**, 4307–4315 (2019).
72. Suzuki, H., Kurihara, Y., Kanehisa, T. & Moriwaki, K. Variation in the distribution of silver-staining nucleolar organizer regions on the chromosomes of the wild mouse, *Mus musculus*. *Mol. Biol. Evol*. **7**, 271–282 (1990).
73. Kurihara, Y., Suh, D. S., Suzuki, H. & Moriwaki, K. Chromosomal locations of Ag-NORs and clusters of ribosomal DNA in laboratory strains of mice. *Mamm. Genome* **5**, 225–228 (1994).
74. Strongin, D. E., Groudine, M. & Politz, J. C. R. Nucleolar tethering mediates pairing between the IgH and Myc loci. *Nucleus* **5**, 474–481 (2014).
75. Jonkers, I., Kwak, H. & Lis, J. T. Genome-wide dynamics of Pol II elongation and its interplay with promoter proximal pausing, chromatin, and exons. *eLife* **3**, e02407 (2014).
76. Dileep, V. & Gilbert, D. M. Single-cell replication profiling to measure stochastic variation in mammalian replication timing. *Nat. Commun*. **9**, 427 (2018).
77. Bacher, R. et al. SCnorm: robust normalization of single-cell RNA-seq data. *Nat. Methods* **14**, 584–586 (2017).
78. Vallejos, C. A., Risso, D., Scialdone, A., Dudoit, S. & Marioni, J. C. Normalizing single-cell RNA sequencing data: challenges and opportunities. *Nat. Methods* **14**, 565–571 (2017).
79. Hafemeister, C. & Satija, R. Normalization and variance stabilization of single-cell RNA-seq data using regularized negative binomial regression. *Genome Biol*. **20**, 296 (2019).
80. Traag, V. A., Waltman, L. & van Eck, N. J. From Louvain to Leiden: guaranteeing well-connected communities. *Sci. Rep*. **9**, 5233 (2019).
81. Stuart, T. et al. Comprehensive integration of single-cell data. *Cell* **177**, 1888–1902 (2019).
82. Serrano, L. et al. The tumor suppressor SirT2 regulates cell cycle progression and genome stability by modulating the mitotic deposition of H4K20 methylation. *Genes Dev*. **27**, 639–653 (2013).
83. Hastie, T. & Stuetzle, W. Principal curves. *J. Am. Stat. Assoc*. **84**, 502–516 (1989).
84. Haghverdi, L., Büttner, M., Wolf, F. A., Buettner, F. & Theis, F. J. Diffusion pseudotime robustly reconstructs lineage branching. *Nat. Methods* **13**, 845–848 (2016).
85. van Dijk, D. et al. Recovering gene interactions from single-cell data using data diffusion. *Cell* **174**, 716–729 (2018).
86. Angerer, P. et al. destiny: diffusion maps for large-scale single-cell data in R. *Bioinformatics* **32**, 1241–1243 (2016).
87. Shannon, P. et al. Cytoscape: a software environment for integrated models of biomolecular interaction networks. *Genome Res*. **13**, 2498–2504 (2003).
88. Lyon, M. F. X-chromosome inactivation: a repeat hypothesis. *Cytogenet. Cell Genet*. **80**, 133–137 (1998).
89. Meuleman, W. et al. Constitutive nuclear lamina-genome interactions are highly conserved and associated with A/T-rich sequence. *Genome Res*. **23**, 270–280 (2013).

Acknowledgements We thank I. Strazhnik for help with figures; A. Anderson for help with the manuscript; C. Karp for custom-made flow cells; H. -J. Ahn for the early phase of the antibody conjugation; and B. Bonev for the Hi-C data. This project is funded by NIH 4DN DA047732 and supplement, and the Paul G. Allen Frontiers Foundation Discovery Center.

Author contributions Y.T. and L.C. conceived the idea and designed experiments. Y.T. designed probes with help from J.T. and C.-H.L.E. Y.T. and J.Y. prepared and validated all the experimental materials. Y.T. performed all the experiments with help from J.Y. Y.T. and N.P. performed image analysis with help from J.W. and S. Shah. Y.T., S.Z. and L.C. analysed data with N.O. and S. Suo. L.C., M.G. and G.-C.Y. supervised the analysis process. Y.T. and L.C. wrote the manuscript with input from C.-H.L.E. and G.-C.Y. L.C. supervised all aspects of the projects.

Competing interests L.C. is a co-founder of Spatial Genomics Inc.

Additional information

Supplementary information The online version contains supplementary material available at https://doi.org/10.1038/s41586-020-03126-2.

Correspondence and requests for materials should be addressed to L.C.

Peer review information *Nature* thanks Peter Fraser and the other, anonymous, reviewer(s) for their contribution to the peer review of this work. Peer reviewer reports are available.

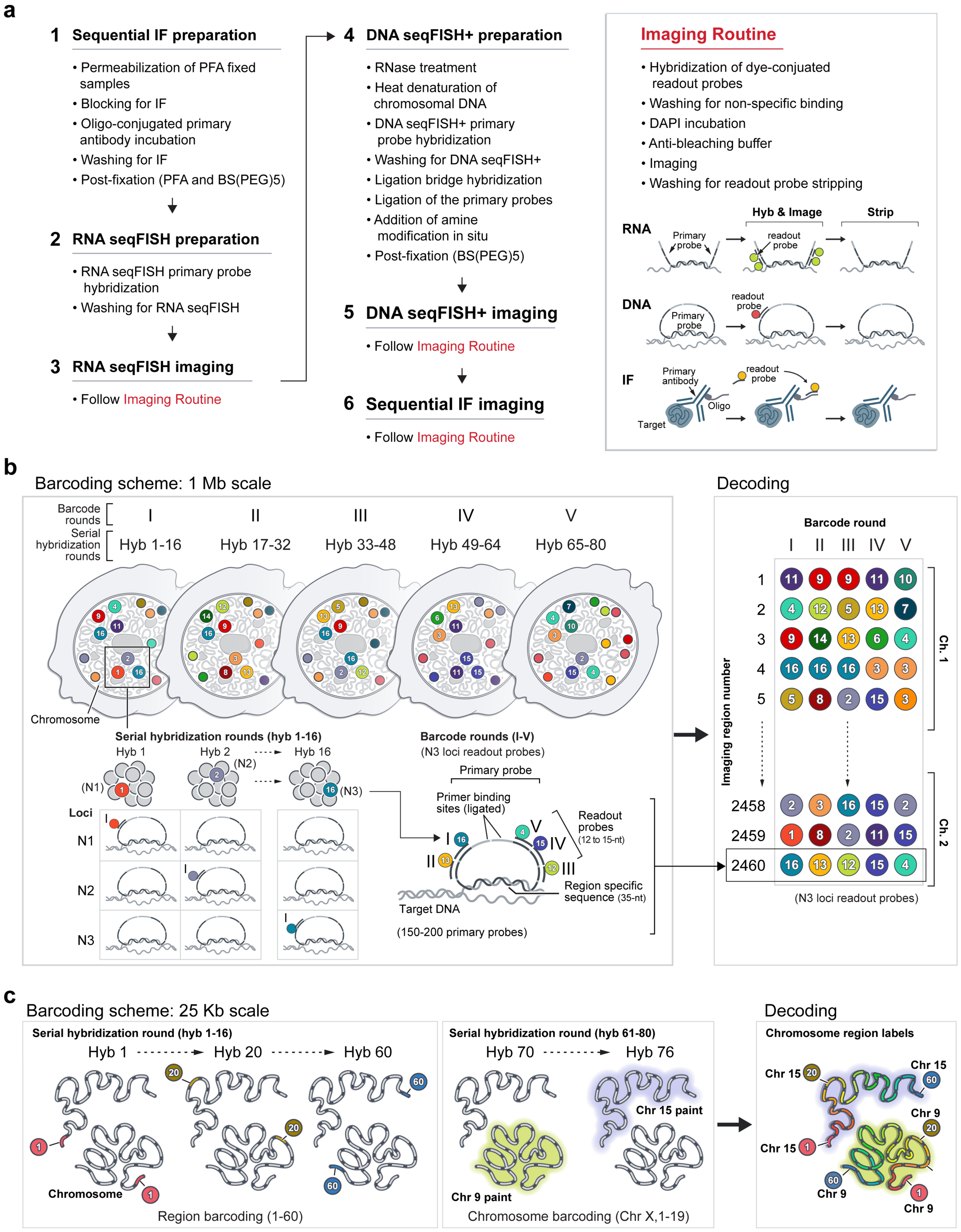

1 Sequential IF preparation

- Permeabilization of PFA fixed samples
- Blocking for IF
- Oligo-conjugated primary antibody incubation
- Washing for IF
- Post-fixation (PFA and BS(PEG)5)

2 RNA seqFISH preparation

- RNA seqFISH primary probe hybridization
- Washing for RNA seqFISH

3 RNA seqFISH imaging

- Follow Imaging Routine

4 DNA seqFISH+ preparation

- RNase treatment
- Heat denaturation of chromosomal DNA
- DNA seqFISH+ primary probe hybridization
- Washing for DNA seqFISH+
- Ligation bridge hybridization
- Ligation of the primary probes
- Addition of amine modification in situ
- Post-fixation (BS(PEG)5)

5 DNA seqFISH+ imaging

- Follow Imaging Routine

6 Sequential IF imaging

- Follow Imaging Routine

Imaging Routine

- Hybridization of dye-conjuated readout probes
- Washing for non-specific binding
- DAPI incubation
- Anti-bleaching buffer
- Imaging
- Washing for readout probe stripping

Imaging region number	I	II	III	IV	V
1	11	9	9	11	10
2	4	12	5	13	7
3	9	14	13	6	4
4	16	16	16	3	3
5	5	8	2	15	3
2458	2	3	16	15	2
2459	1	8	2	11	15
2460	16	13	12	15	4

Extended Data Fig. 1 | See next page for caption.

Extended Data Fig. 1 | Detailed schematics of the integrated spatial genomics approach with DNA seqFISH+, RNA and intron seqFISH and multiplexed immunofluorescence. a, Flow chart of the experimental procedures. Samples are fixed with paraformaldehyde, followed by oligonucleotide-conjugated primary antibody incubation, post-fixation with paraformaldehyde and BS(PEG)5, and RNA seqFISH. Then samples are prepared for DNA seqFISH+. This optimized protocol ensures good alignment between DNA seqFISH+ data with RNA seqFISH and the multiplexed immunofluorescence data on a voxel by voxel level (Extended Data Fig. 2). Bottom right cartoon shows imaging routine for RNA FISH and DNA seqFISH+ with primary probes and sequential immunofluorescence with oligonucleotide-conjugated primary antibodies. **b**, Schematics of DNA seqFISH+ for the 1-Mb resolution dataset. Five rounds of barcoding allows 2,048 barcodes to be detected with 2 rounds of dropout error correction in each fluorescent channel. Two fluorescent channels are used to cover a total of 2,460 loci, spaced approximately 1 Mb apart in the genome. In each round of barcoding, 16 rounds of hybridization are performed to generate 16 pseudocolors. DNA dots detected in each pseudocolor channel are fitted in 3D to determine their super-resolved centroid location and compiled across all 16 pseudocolors to generate a super-resolved localization image. With 5 rounds of barcoding (overall 80 rounds of serial hybridizations), the identity of all DNA loci are decoded. Every DNA locus should appear once in every barcoding round in a single pseudocolor. The barcoding table (Supplementary Table 2) is shown on the right. DNA seqFISH+ probes contain all 5 rounds of barcode readout sequences. Each sequence, for a given barcoding round, has a possible choice of 16 sequences, corresponding to one of the pseudocolors. For each gene, 5 out of the 80 hybridizations will result in hybridization events and fluorescent readout probes bound on the primary DNA hybridizing probes. To preserve the DNA primary probe on the chromosome over all 80 rounds of hybridizations, the primary probes are padlocked[62,63] onto the chromosomes by T4 DNA ligase at the primer binding sites after the initial hybridization (Methods). **c**, Barcode scheme for the 25-kb resolution DNA seqFISH+. 60 adjacent 25-kb regions are sequentially readout and imaged in 60 rounds of hybridization. This is carried out in parallel on 20 chromosomes. In other words, each round of hybridization images 20 different loci on different chromosomes. An additional 20 rounds of hybridization are carried out to label each chromosome one at a time to assign chromosomal identity to each locus imaged during the first 60 rounds individually. The 1-Mb resolution data were collected in the 643-nm (channel 1) and 561-nm (channel 2) channels in **b**, while the 25 kb resolution data were collected in the 488-nm channel (channel 3) in **c**.

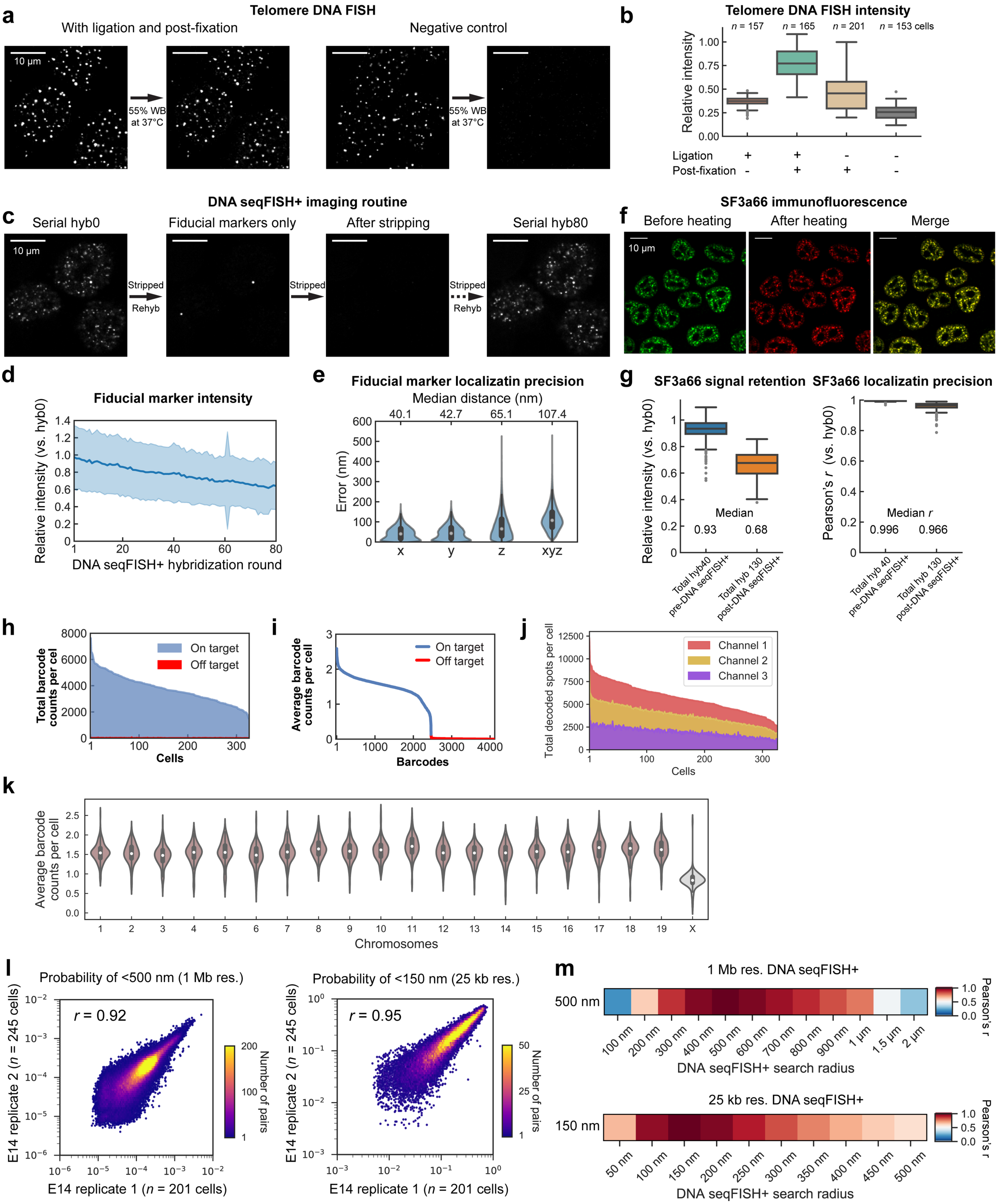

Extended Data Fig. 2 | See next page for caption.

Extended Data Fig. 2 | Optimization and validation for DNA seqFISH+. **a**, Ligation and post-fixation of primary probes prevent their dissociation at the readout probe stripping step, validated by telomere DNA FISH. 55% formamide wash buffer (WB) solution at 37 °C was added to the cells for 16 h with and without the primary probes padlocked[62,63] onto the chromosomal DNA. Probes were retained in the ligated sample, and not retained in the unligated sample. Note that 55% WB was used at room temperature for 2 min in each stripping step during the seqFISH routine, which is less stringent than the condition used here. **b**, Quantification of the signal retention after the harsh wash in **a**, with telomere DNA FISH across multiple conditions. Total intensities in individual nuclei from a single *z*-section were compared before and after the harsh wash. In the DNA seqFISH+ experiments, the condition with ligation and post-fixation was used. The number of cells from two independent measurements is written in the plot. For the box plots in **b** and **g**, the centre line in the boxes marks median, the upper and lower limits of the boxes mark the interquartile range, the whiskers extend to the farthest data points within 1.5 times the interquartile range, and the grey points mark outliers. **c**, Primary probes are still bound after more than 81 rounds of hybridization, and the specific signals return in the DNA seqFISH+ experiments. Initial hyb0 for DNA seqFISH+ was performed with hyb80 readout probes for comparison. Fiducial markers targeting a repetitive region of the genome with a single primary probe were also imaged initially and included in all 80 imaging rounds for alignment. **d**, Quantification of the fiducial marker intensities for 80 hybridization rounds in the DNA seqFISH+ experiments, relative to that from hyb0 fiducial markers. Fiducial markers ($n = 506$-1,117 dots per hybridization round) from 446 cells in DNA seqFISH+ experiments were used for quantification. Shaded regions represent the mean (centre) with s.d. **e**, Localization errors of fiducial markers across hyb 1 to 80 in the DNA seqFISH+ experiments, $n = 71{,}981$ aligned spots for x and y, and $n = 87{,}879$ aligned spots for z from 446 cells in DNA seqFISH+ experiments. For x and y alignments, we filtered out aligned dots that were more than 2× s.d. away from the mean displacement at each hybridization, and new alignments were computed. **f**, Preservation of the nuclear structure through the double fixation procedure. Good colocalization (yellow in the right panel) of the nuclear speckles (SF3A66) before and after heating. **g**, Quantification of the SF3A66 immunofluorescence signal retention in the nuclei (left) and localization precision (right) measured by Pearson correlation of pixel intensities in the nuclei with a single *z*-section between hyb0 (pre-DNA seqFISH+ steps) image and hyb40 (pre-DNA seqFISH+ steps) or hyb130 (post-DNA seqFISH+ steps). $n = 326$ cells in the centre field of views from two DNA seqFISH+ biological replicates in **g**–**k**. **h**, Frequencies of on- and off-target barcodes in channel 1 and 2 per cell. On average, 3,636.0 ± 1,052.6 (median ± s.d.) on-target barcodes and 14.0 ± 7.4 off-target barcodes are detected per cell ($n = 326$ cells from the centre field of views of the two biological replicates). **i**, Average frequencies of individual on-target and off-target barcodes ($n = 4{,}096$ barcodes in channel 1 and 2), demonstrating the accuracy of the DNA seqFISH+. **j**, The total number of dots detected in each of the fluorescent channels in single cells. Channels 1 and 2 contain the 1-Mb data and channel 3 contains the 25-kb data. **k**, The average number of dots detected per each locus per cell across all 20 chromosomes. Note that 2 dots per cell are not 100% detection efficiency because some cells are in the G2 phase of the cell cycle (4 alleles in total). X chromosome has half the number of dots detected per locus (0.84 ± 0.21 (median ± s.d.)) compared with the other autosomes (1.57 ± 0.27), because E14 mouse ES cells are a male diploid cell line (Methods). **l**, Pearson correlation of probabilities for the pairs of loci within a search radius of 500 nm (1-Mb data) and 150 nm (25-kb data) between two biological replicates of DNA seqFISH+ experiments. All unique intra-chromosomal pairs of loci were calculated for the 1-Mb ($n = 2{,}460$ loci) and 25-kb data ($n = 1{,}200$ loci) with $n = 201, 245$ cells for biological replicates 1 and 2, respectively. **m**, PCC of the proximity probability between loci pairs as a function of search radii in comparison to 500-nm search radius (1-Mb data) and 150-nm search radius (25-kb data) used in **l**. $n = 446$ cells from the two DNA seqFISH+ biological replicates.

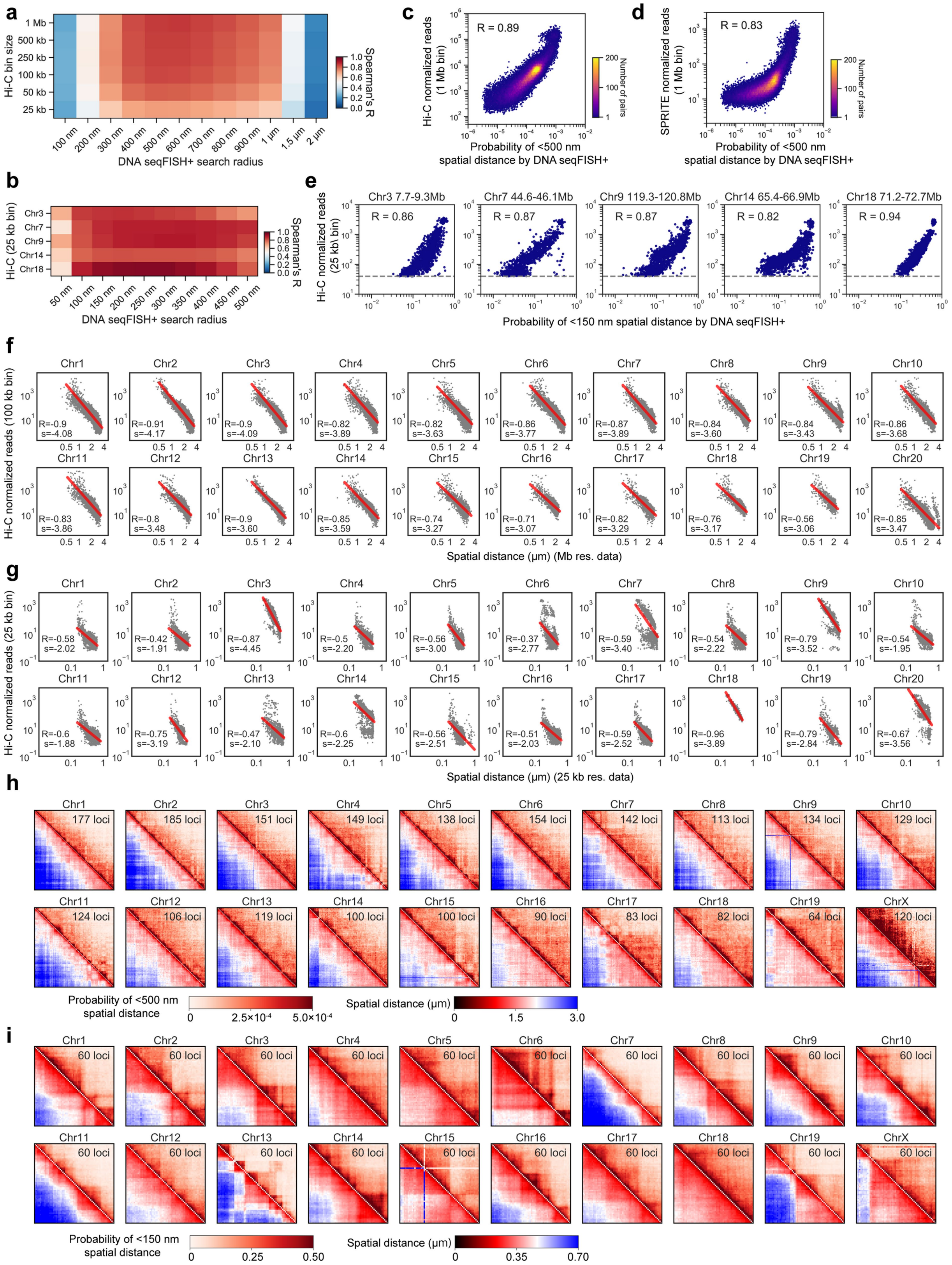

Extended Data Fig. 3 | See next page for caption.

Extended Data Fig. 3 | Additional validation for DNA seqFISH+. **a**, **b**, Spearman correlation between probabilities of pairs of loci within a search radius of 100 nm–2 µm by DNA seqFISH+ and frequencies by Hi-C[23] in mouse ES cells with a certain bin size. All unique intra-chromosomal pairs of loci were calculated for the 1-Mb ($n = 2,340$ autosomal loci) and 25-kb data ($n = 60$ loci per chromosome), and overlapping regions within the bin in **a** were excluded from this analysis. At 1.5 Mb chromosomal regions with 25 kb resolution in **b**, median Hi-C reads vary depending on the 1.5 Mb regions targeted, ranging from 0.9 to 203.2. We used 5 autosomal regions with Hi-C reads greater than 40 per 25-kb bin for comparison. **c**, Comparison of probabilities within 500-nm search radius for intra-chromosomal locus pairs in autosomes in DNA seqFISH+ (1-Mb resolution data) and the frequencies in Hi-C[23] data in mouse ES cells. Spearman correlation coefficient of 0.89 computed from $n = 84,707$ unique intra-chromosomal pairwise combinations. Hi-C data were binned with 1-Mb data, and overlapping regions within 1 Mb were excluded from this analysis. **d**, Comparison of probabilities within a 500-nm search radius for the intra-chromosomal locus pairs in autosomes by DNA seqFISH+ (1-Mb resolution data) and frequencies by SPRITE[7] in mouse ES cells. Spearman correlation coefficient of 0.83. The same binning and filtering were used as the Hi-C analysis in **c**. **e**, Comparison of probabilities within 150-nm search radius for the locus pairs in the selected autosomes by DNA seqFISH+ (25-kb resolution data) and frequences by Hi-C[23] in mouse ES cells. Spearman correlation coefficients ranged from 0.82 to 0.94 computed from $n = 948$–1,776 unique pairwise combinations, using the same selection and filtering criteria as **b**. **f**, **g**, Relationships between median spatial distance of pairs of loci for 1-Mb resolution data in **f** and 25-kb resolution data in **g** by DNA seqFISH+ and Hi-C frequencies. The red lines are power-law fits with fitting parameters S shown with Spearman correlation coefficient R. **h**, **i**, Heat maps showing probabilities of pairs of loci within a search radius of 500 nm in **h** and 150 nm in **i** (top right triangles), and median spatial distances of pairs of loci (bottom left triangles) in each chromosome for 1 Mb resolution data in **h** and 25-kb resolution data in **i** by DNA seqFISH+. $n = 446$ cells from two biological replicates for DNA seqFISH+ data in **a**–**i**.

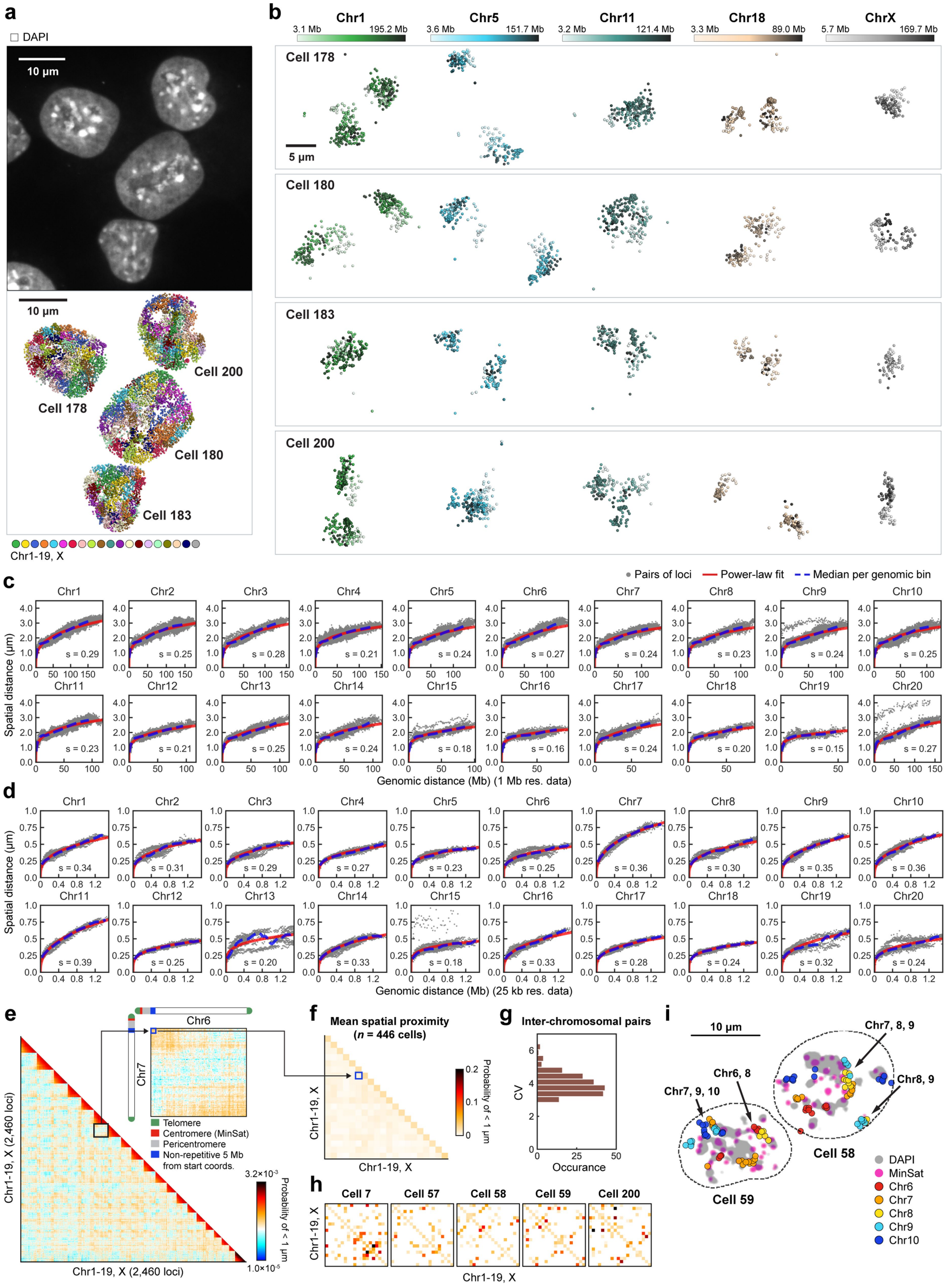

Extended Data Fig. 4 | See next page for caption.

Extended Data Fig. 4 | Single-cell organization and physical scaling of chromosomes by DNA seqFISH+. a, DAPI staining image of mouse ES cells (top) and 3D image of corresponding nuclei with individual chromosomes labelled with different colours (bottom). **b**, 3D image of individual chromosomes, coloured based on chromosome coordinates (light to dark colours). Chromosomes are from cells in **a**. The images are representative of *n* = 446 cells profiled with DNA seqFISH+. **c**, **d**, Scaling of median spatial distance as a function of genomic distance for 20 chromosomes with 1-Mb resolution data in **c** and 25-kb resolution data in **d**. Grey dots represent the median distance of the given pairs of loci. Blue dashed lines are the median spatial distance at each genomic distance bin, while red lines are power-law function fits with the fitting parameters in the plots. *n* = 446 cells. **e**, The full spatial proximity map between all loci from the 1-Mb DNA seqFISH+ data with a search radius of 1 μm (bottom left triangle panel). The zoomed in view of the map for chr6 and chr7 (top right panel), showing the non-repetitive regions near pericentromeric repetitive regions from different chromosomes are more likely to be spatially close to each other. Colour bar is shown in log scale. **f**, Mean spatial proximity map for 20 chromosomes, considering only the first 5 Mb non-repetitive regions in each chromosome with a search radius of 1 μm. **g**, Distribution of coefficient of variation (CV) for spatial proximity from inter-chromosomal pairs in **f**. **h**, Single cell version of spatial proximity maps in **f** show heterogeneity in the spatial proximity between the proximal 5 Mb non-repetitive regions of the chromosomes. **i**, Single nuclei image shows that proximal 5 Mb non-repetitive regions from only a subset of chromosomes appear near the DAPI-rich pericentromeric heterochromatin regions in individual nuclei. The images are representative of *n* = 446 cells and the analysis are quantified from 2 biological replicates in **e**–**h**.

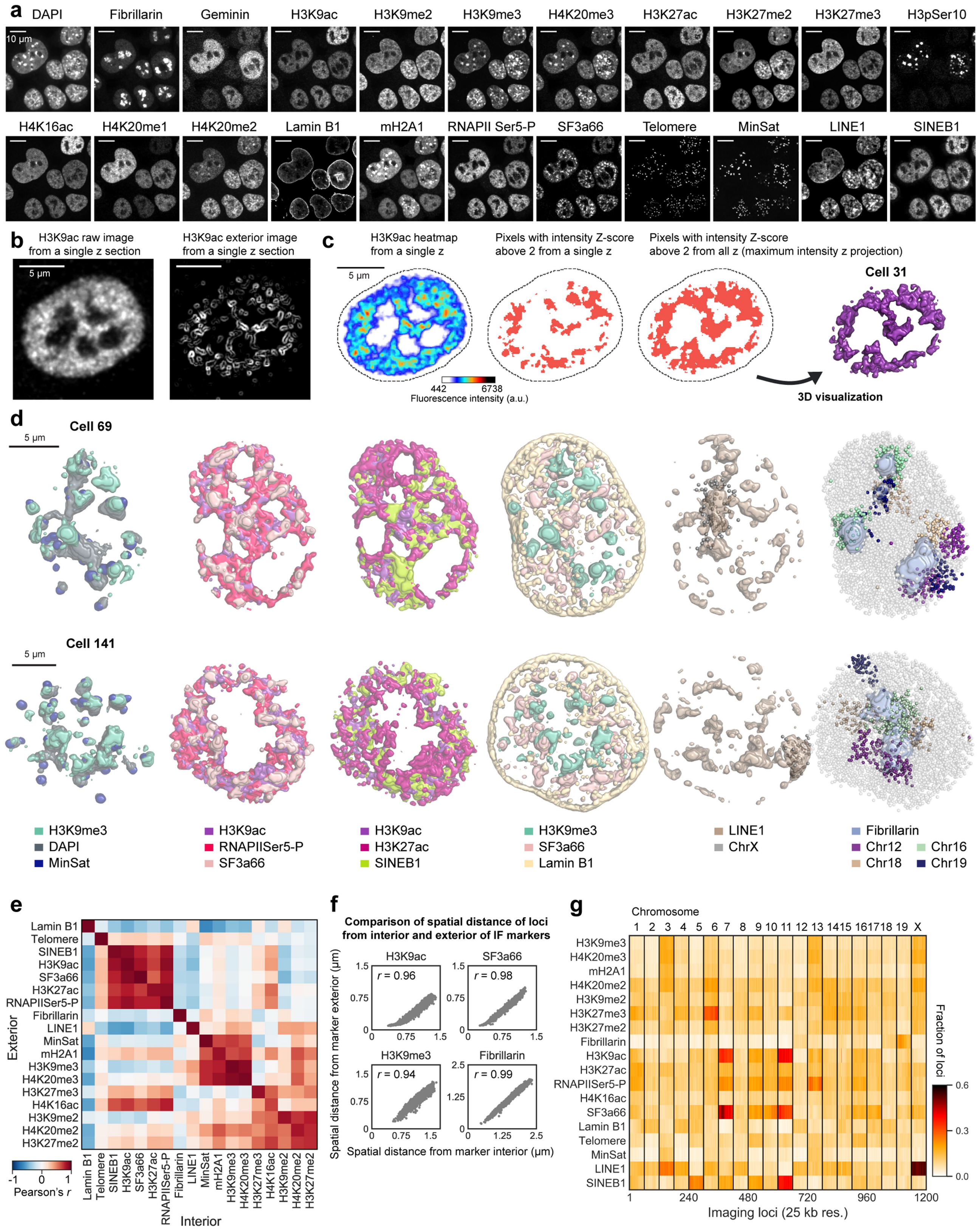

Extended Data Fig. 5 | See next page for caption.

Extended Data Fig. 5 | Visualization and validation for sequential immunofluorescence and repetitive element DNA FISH. **a**, 17 antibodies and 4 repetitive elements, including gene-poor long interspersed nuclear elements (LINE1), gene-rich short interspersed nuclear elements (SINEB1), centromeric MinSat, and telomeres, are imaged along with DAPI. Individual cells have different patterns of immunofluorescence staining. Note that the DAPI patterns are not identical between cells. Similarly, marks that are colocalized with DAPI-rich pericentromeric heterochromatin regions are different between cells and even between different pericentromeric regions in a single cell. **b**, Representative H3K9ac image and edge-transformed image that detects the voxels on the exterior of H3K9ac globules (Methods). **c**, Representative H3K9ac images from a single *z*-section or maximum intensity *z*-projection with the intensity *Z*-score threshold above 2. 3D visualization (right) was performed for the pixels with the intensity *Z*-score above 2 (Methods). **d**, Additional single cell 3D images of immunofluorescence markers for the pixels with the intensity *Z*-score above 2. Heterochromatin components (H3K9me3, DAPI and MinSat) were clustered together, while RNAPIISer5-P, active marks (H3K9ac, H3K27ac), SINEB1 and nuclear speckles (SF3A66) were physically proximal. High intensity pixels of LINE1 by DNA FISH localized mainly to the LINE1-rich X chromosome[88]. **e**, Correlation of chromatin profiles for all 2,460 loci at 1 Mb resolution generated from distance to the interior and exterior voxels of different immunofluorescence marks ($n = 446$ cells). **f**, Scatter plots of the distances from each locus to interior voxels versus exterior voxels that are 2× s.d. above the mean for 2,460 loci at 1-Mb resolution ($n = 446$ cells). PCCs are shown. **g**, Heat map showing fraction of loci within 300 nm from immunofluorescence marks and repetitive elements by DNA seqFISH+ at 25-kb resolution ($n = 1,200$ loci and 446 cells).

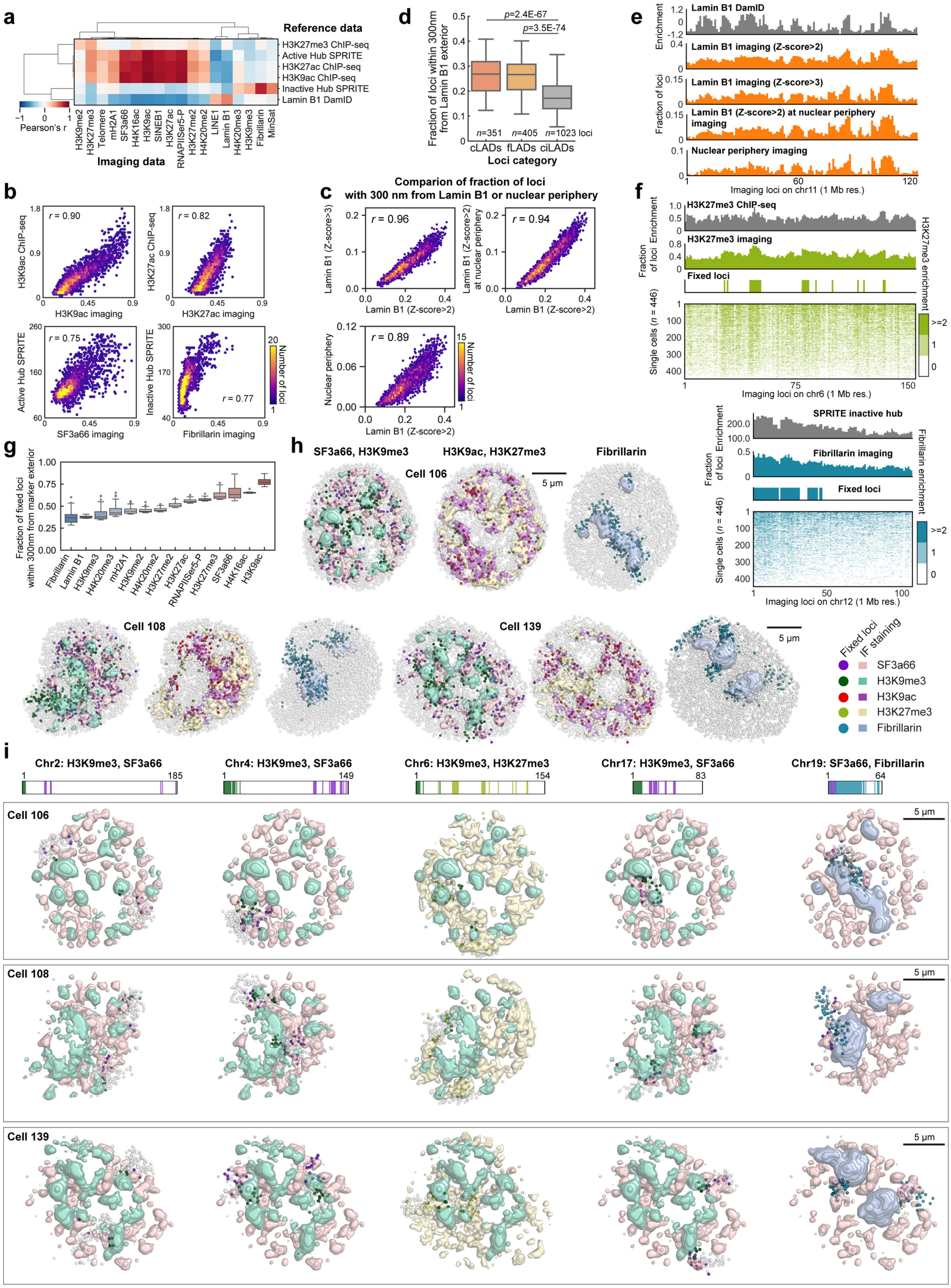

Extended Data Fig. 6 | See next page for caption.

Extended Data Fig. 6 | Additional visualization and validation for fixed loci and chromatin profiles. **a**, Correlation matrix comparing the chromatin profiles by DNA seqFISH+ and immunofluorescence with other methods[7,24,35]. The 1-Mb DNA seqFISH+ data were used and the reference data were binned with 1-Mb data. Chromatin profiles were computed as the fraction of loci within 300 nm from immunofluorescence marker exterior for the 2,460 loci (*n* = 446 cells). **b**, Two-dimensional density plots of individual marker comparison shown in **a**. *n* = 2,460 loci. **c**, Comparison of fraction of loci within 300 nm from the lamin B1 exterior with different thresholding values (*Z*-score above 2 or 3), or from nuclear periphery computed from convex hull of nuclear pixels (Methods), showing the good agreement of the profiles in different quantification criteria (*n* = 2,460 loci from 446 cells). **d**, Validation of lamin B1 enrichment with loci categorized as cell-type invariant constitutive lamina-associated domains (cLADs), cell-type dependent facultative LADs (fLADs), and constitutive inter-LADs (ciLADs) assigned from previous DamID studies[35,89]. Loci categorized as both cLADs and fLADs show enrichment of proximities to lamin B1 compared to those from ciLADs, representing a good agreement of our measurement (*n* = 351, 405 and 1,023 loci in cLADs, fLADs, ciLADs, respectively, category averaged from 446 cells) with the DamID studies. n is the number of loci. For the box plots in **d** and **g**, the centre line in the boxes marks median, the upper and lower limits of the boxes mark the interquartile range, the whiskers extend to the farthest data points within 1.5 times the interquartile range, and the grey points mark outliers. **e**, Additional visualization for chromatin profiles of Lamin B1 with different criteria in **c** (*n* = 446 cells) in comparison with Lamin B1 DamID profile[35]. To take into account only Lamin B1 staining at the nuclear periphery, we calculated the distances between the DNA loci and the Lamin B1 signal near the convex hull of the nucleus as well as with different intensity thresholds. **f**, Additional examples for single cell chromatin profiles in comparison with ChIP–seq[24] for H3K27me3 (top) and SPRITE[7]. The profiles were computed and are displayed in the same way as Fig. 2c. *n* = 446 cells. **g**, The fraction of loci in single cells that are associated with exteriors of immunofluorescence markers for the fixed loci defined based on the chromatin profiles (*n* = 446 cells). Note that different immunofluorescence markers have different thresholds for calling fixed loci. Thus, fixed loci for some immunofluorescence markers are more consistently associated with the immunofluorescence marks in single cells. **h**, Additional 3D images of immunofluorescence markers and their associated fixed loci. In each cell, 6 immunofluorescence marks (2 per panel) are shown for visual clarity. **i**, 5 chromosomes are highlighted in the 3 cells shown in **h**. The fixed loci for a pair of immunofluorescence markers are shown for each chromosome in the corresponding image visualization. Fixed loci are shown in colored dots and the remaining loci on the chromosomes are shown as grey dots. The same colour codes are used in **h**.

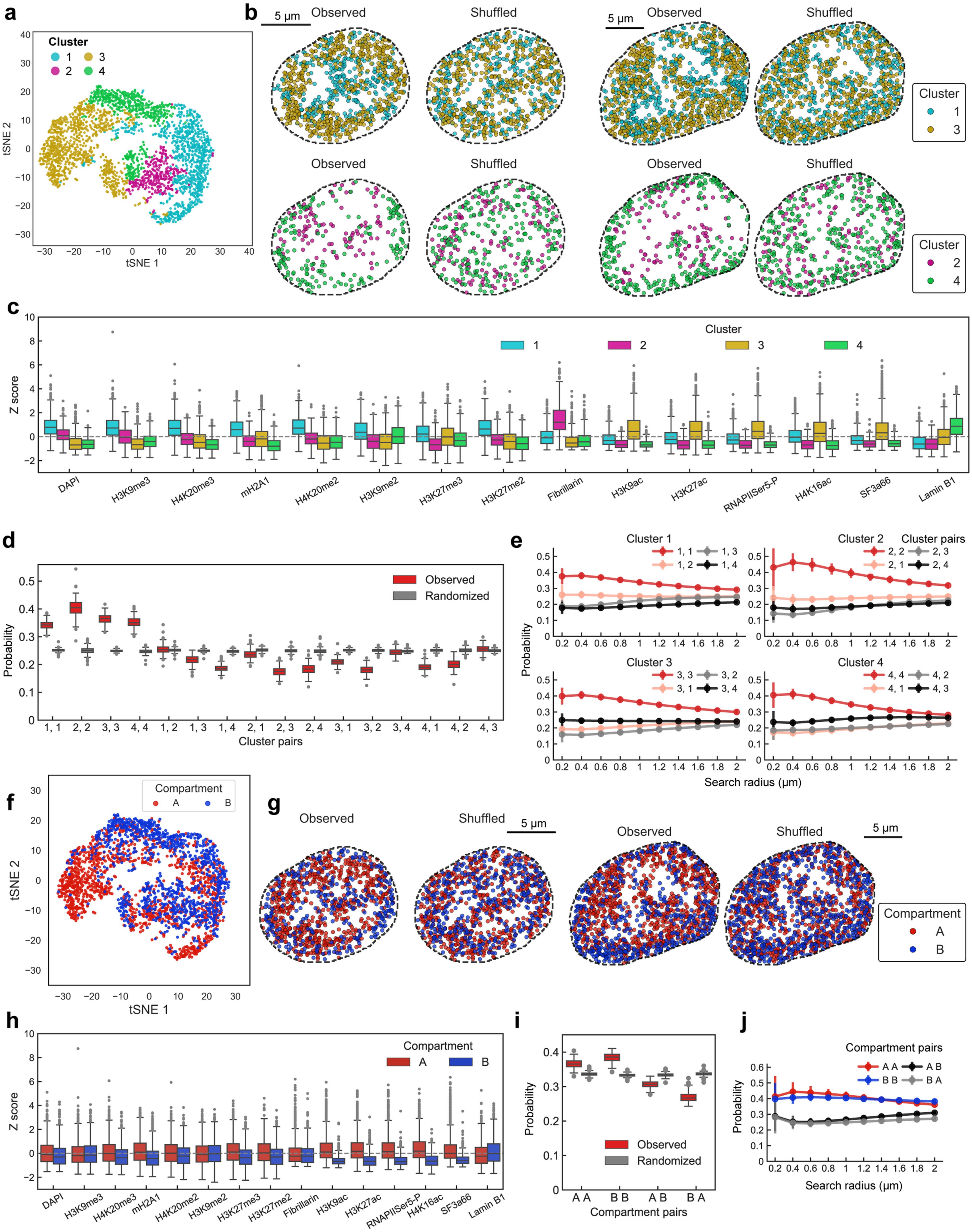

Extended Data Fig. 7 | See next page for caption.

Extended Data Fig. 7 | Comparison between population level and single cell level chromosome organization in association with chromatin markers. **a**, Clustering of the ensemble-averaged immunofluorescence spatial proximity profile of individual loci. $n = 2{,}460$ loci ($n = 805, 278, 877, 500$ loci in each cluster, respectively). **b**, In individual cells, loci associated with each cluster are mapped onto their spatial location. Note that cluster definitions for DNA loci were obtained from population-averaged data, and those cluster-assigned loci distribution may not necessarily reflect immunofluorescence marker localization in single cells. **c**, Box plot of immunofluorescence marks for the loci in each of the clusters. Cluster 1 is enriched in repressive markers such as H3K9me3, mH2A1, DAPI. Cluster 2 is enriched in interactions with fibrillarin. Cluster 3 is enriched in active marks such as RNAPII(Ser5P), H3K27ac and SF3A66 (nuclear speckle marker). Cluster 4 is enriched in lamin B1. For the box plots in **c**, **d**, **h**, **i**, the centre line in the boxes marks median, the upper and lower limits of the boxes mark the interquartile range, the whiskers extend to the farthest data points within 1.5 times the interquartile range, and the grey points mark outliers. **d**, The probability of loci of certain cluster pairs within 1 µm search radius in individual cells. Cluster definitions follow those in **a**–**c**. Randomized data were generated by scrambling the cluster identities of individual loci in cells while keeping the total number of loci within each cluster the same within that cell. The probability for observed and randomized data for each cell are shown as box plots. **e**, The probability that pairs of loci with cluster assignments are found within a given search radius, as a function of search radius. Error bars represent standard error over 20 bootstrap trials. **f**, Mapping of the A/B compartment definitions[23] onto the *t*-SNE plot based on the ensemble-averaged loci-immunofluorescence mark spatial proximity map. Note that regions that are not assigned to one of the compartments were excluded from the analysis. ($n = 1{,}188$ and 960 loci in A and B compartments, respectively). **g**, Reconstructions of individual cells with loci assigned as A or B compartment mapped onto their spatial location. Observed compared to randomized data for 2 cells shown in **b**. **h**, Box plot of the immunofluorescence marks for the loci assigned to A or B compartments. **i**, The probability that loci in A/B compartments are within 1 µm search radius in individual cells, similar to **d**. **j**, The probability that pairs of loci with A/B assignments are found within a given search radius, as a function of search radius for spatial proximity, similar to **e**. $n = 446$ cells from two biological replicates in **a**–**j**.

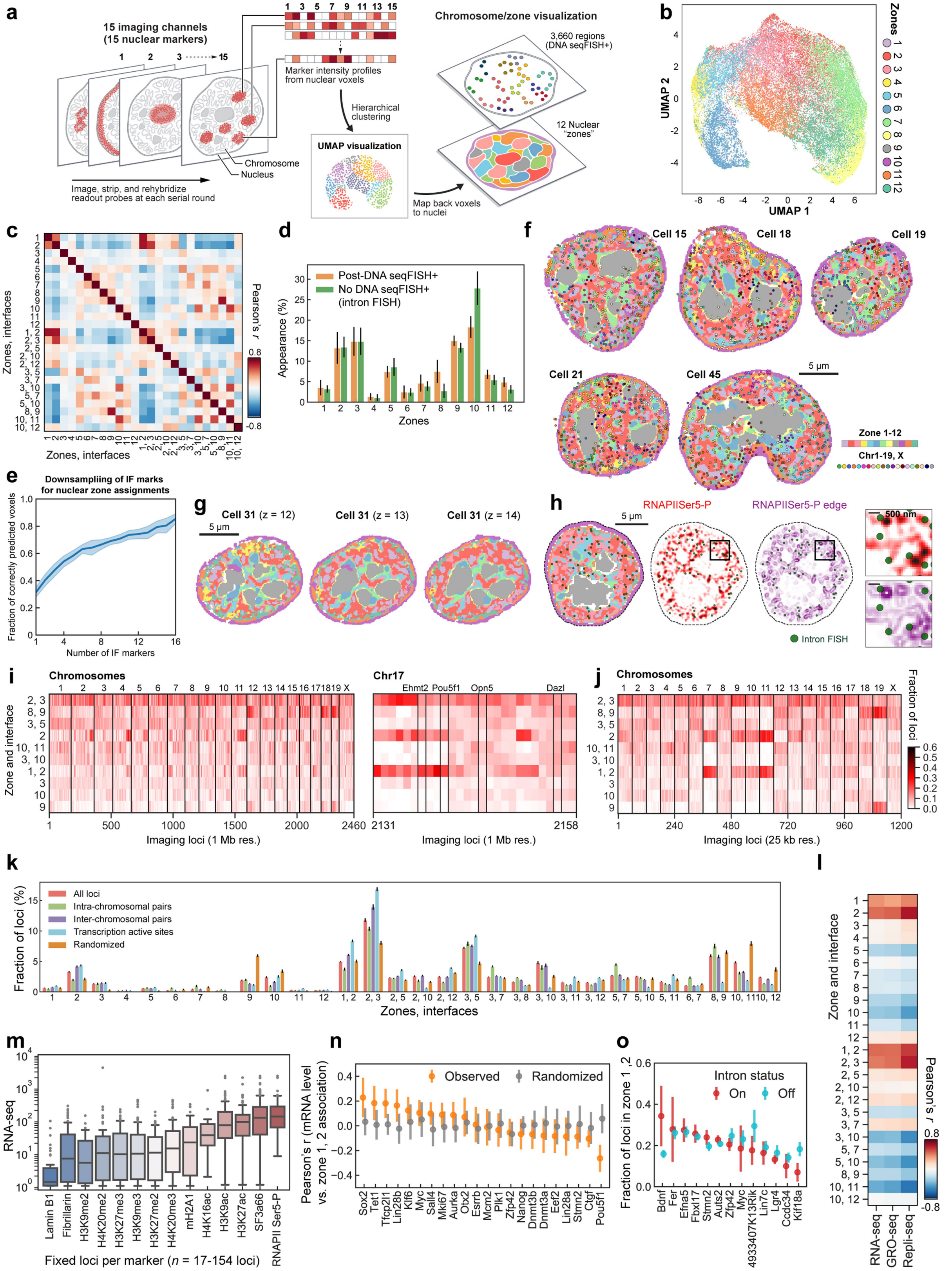

Extended Data Fig. 8 | See next page for caption.

Extended Data Fig. 8 | Further characterization of nuclear zones and interfaces. a, Analysis workflow for the pixel-based combinatorial chromatin profiling. Individual voxels with the 15 chromatin markers are clustered with hierarchical clustering and visually represented by a nonlinear dimensionality reduction technique (UMAP)[70]. Voxels from individual clusters (zones) are mapped back to individual nuclei, and overlaid with DNA seqFISH+ dots. **b**, UMAP representation for 44,000 pixels sampled from 201 cells, labelled with 12 zones. UMAP projection is used for visual clarity. **c**, Pearson correlation matrix between zones and interfaces based on the DNA loci association with zones and interfaces shown in **f** (n = 2,460 loci). Loci appearing in zone 1 are also more likely to be found in zone 2 as well as in interface 1/2. **d**, Comparison of zone appearance with and without DNA seqFISH+ treatment shows an overall agreement between the measurements. Mean values from 20 bootstrap trials are shown with error bars corresponding to standard errors. **e**, Assignment of zones as a function of downsampling of immunofluorescence markers. Twenty random subsets of immunofluorescence markers are selected at each downsample size. The centre of the curve reflects the mean and the width reflects the standard deviation of the correct zone assignments at each downsample size (Methods). **f**, Reconstructions of zones and DNA loci in additional cells. **g**, Reconstructions of zones in the cell 31 with different *z*-planes. **h**, Reconstruction of zones and 1,000-gene intron dots as well as RNAPIISer5-P staining (background-subtracted) and edge of RNAPIISer5-P staining. **i**, Heat map for probability of association between DNA loci, nuclear zones and interfaces for the 1-Mb data. Zones and interfaces are ordered according to the overall probability of association with DNA loci. Right panel shows the loci around *Pou5f1* visualized in Fig. 3b (panel 1). Each locus in single cells is assigned to one zone or interface. The distribution shown in the heat map reflects the single cell variability in zone association for each locus. For example, *Ehmt2* and *Pou5f1* loci were primarily associated with active zone 2 and interfaces 1/2 and 2/3, whereas *Opn5* and *Dazl* loci were more uniformly distributed across many zones. **j**, Heat map for probability of association between DNA loci, nuclear zones and interfaces for the 25-kb data. Loci within the same Mb region have similar nuclear zone and interface association probability. **k**, Frequency of association between DNA loci and zones or interfaces in single cells, calculated for all loci, loci with intra-chromosomal and interchromosomal pairs, TAS measured by intron FISH, and random loci (randomized control). Mean values from 20 bootstrap trials are shown with error bars corresponding to standard errors. **l**, Correlation between zone association and gene expression levels (RNA-seq)[49], density of RNA polymerases on the loci (GRO-seq)[75] and early replication domains (Repli-seq)[76] for all loci at 1-Mb resolution (n = 2,460 loci). **m**, Expression levels of fixed loci for each immunofluorescence marker from n = 446 cells. Population level expressions are taken from bulk RNA-seq studies[49] and integrated for a 1-Mb region. For the box plots, the centre line in the boxes marks median, the upper and lower limits of the boxes mark the interquartile range, the whiskers extend to the farthest data points within 1.5 times the interquartile range, and the grey points mark outliers. **n**, Correlation of mRNA levels and fraction of voxels within 300 nm of a given locus in single cells being in active zones for individual mRNAs. Mean values from 20 bootstrap trials are shown with error bars corresponding to standard errors for each mRNA. Randomized samples correspond to scrambling of mRNA and zone assignment values for each cell. **o**, Comparison of fraction of voxels within 300 nm of DNA loci to be in active zones (zone 1 and 2) for loci with an active intron signal (ON) versus loci with no intron signal (OFF) for individual introns. Mean values from 20 bootstrap trials are shown with error bars corresponding to standard errors. for each intronic RNA. n = 201 and 172 cells for DNA seqFISH+ and intron FISH measurements in **b**–**l**, **n**, **o**, respectively.

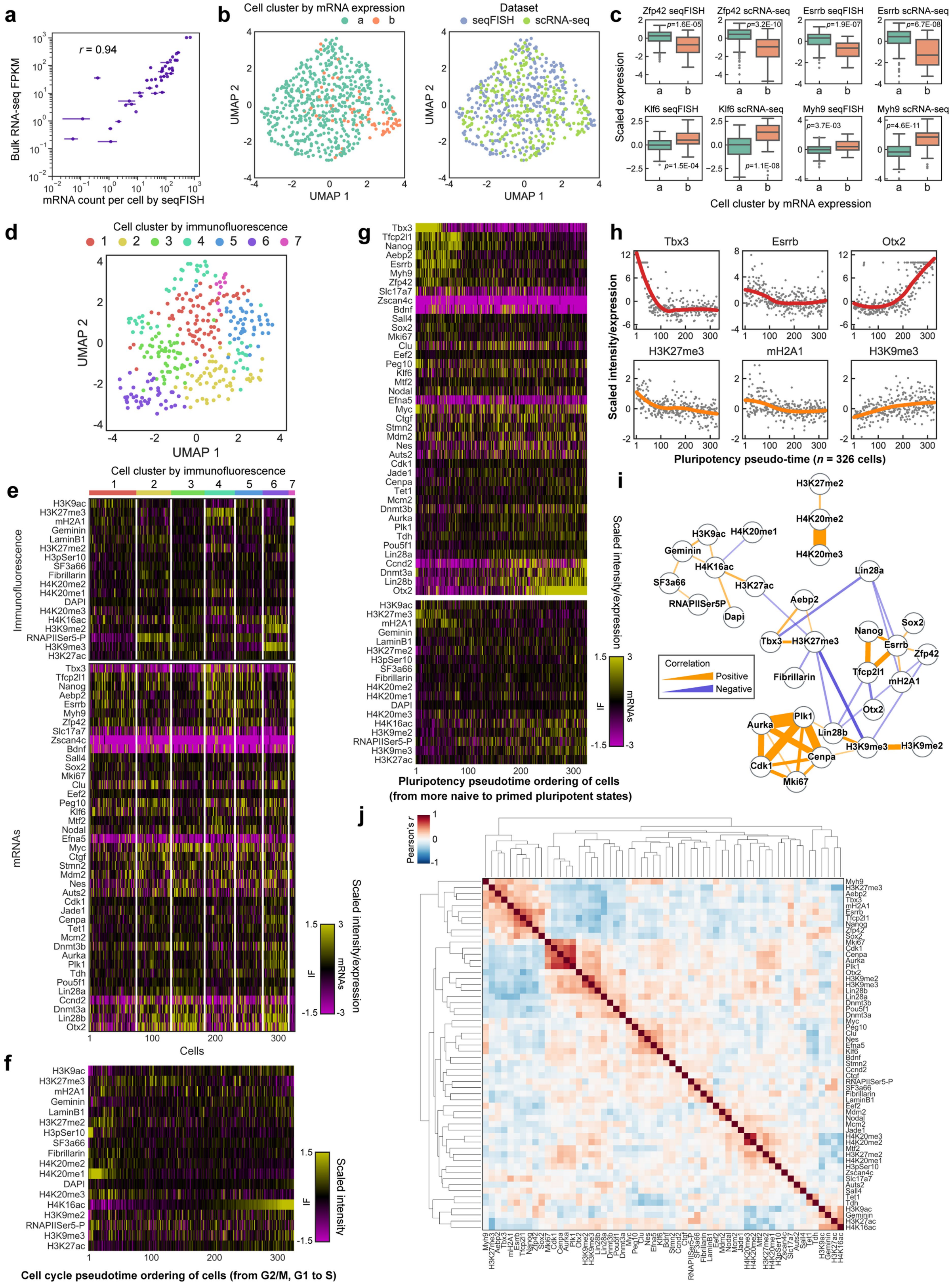

Extended Data Fig. 9 | See next page for caption.

Extended Data Fig. 9 | Heterogeneity of transcriptional and chromatin states and their relationships in single cells. **a**, Pearson correlation of mean mRNA counts by RNA seqFISH and bulk RNA-seq. Error bars for RNA seqFISH represent the standard error of the mean from two measurements ($n = 151$ and 175 cells from the centre field of views). **b**, UMAP representation of individual cells in two different cell clusters identified based on scRNA-seq[42] and mapped onto RNA seqFISH data (cluster a for cells with more pluripotent states and cluster b for cells on the differentiation path) (left), and in different datasets (right) ($n = 326$ and 250 cells for RNA seqFISH and scRNA-seq[42] dataset, respectively). **c**, Box plots showing a good agreement of differentially expressed genes in scRNA-seq and seqFISH datasets. *P* values were from a two-sided Wilcoxon's rank-sum test with cells in clusters a and b ($n = 298$ and 209 cells in cluster a and $n = 28$ and 41 cells in cluster b with RNA seqFISH and scRNA-seq[42] datasets, respectively). For the box plots, the centre line in the boxes marks median, the upper and lower limits of the boxes mark the interquartile range, the whiskers extend to the farthest data points within 1.5 times the interquartile range, and the grey points mark outliers. **d**, UMAP representations of the cell clusters defined by immunofluorescence intensity profiles. **e**, Heat map of cell clusters with distinct immunofluorescence profiles shown with cell cycle associated immunofluorescence markers and all mRNA markers, similar to Fig. 4b. **f**, Pseudotime-course analysis for cell cycle progression, cell cycle markers (H4K16ac, H4K20me1 and H3pSer10) show clear enrichments while other markers do not show specific enrichments upon cell cycle pseudotime course, suggesting majority of the immunofluorescence markers profiled are not primarily affected by cell cycle phases.

g, Pseudotimecourse analysis for pluripotency states in mouse ES cells based on scaled mRNA expression levels, showing the enrichment from markers associated with naive pluripotency such as *Tfcp2l1* and *Nanog* to markers associated with primed pluripotency such as *Dnmt3a*, *Lin28b* and *Otx2* as well as the enrichment of certain chromatin marks upon the pluripotency pseudotime course. **h**, Scaled marker gene expression (top panels) or intensity (bottom panels) along the pluripotency pseudotime ordering of cells. Raw data in **g** are overlaid with fitting curves (Methods). **i**, Network analysis for the mRNA and immunofluorescence markers represents positive and negative Pearson correlation relationships among markers. **j**, Joint Pearson correlation matrix between mRNA and immunofluorescence markers based on the scaled expression or intensity profiles in single cells ($n = 41$ mRNA and 25 immunofluorescence markers). $n = 326$ cells in the centre field of views for RNA seqFISH and immunofluorescence data in **a**–**j**.

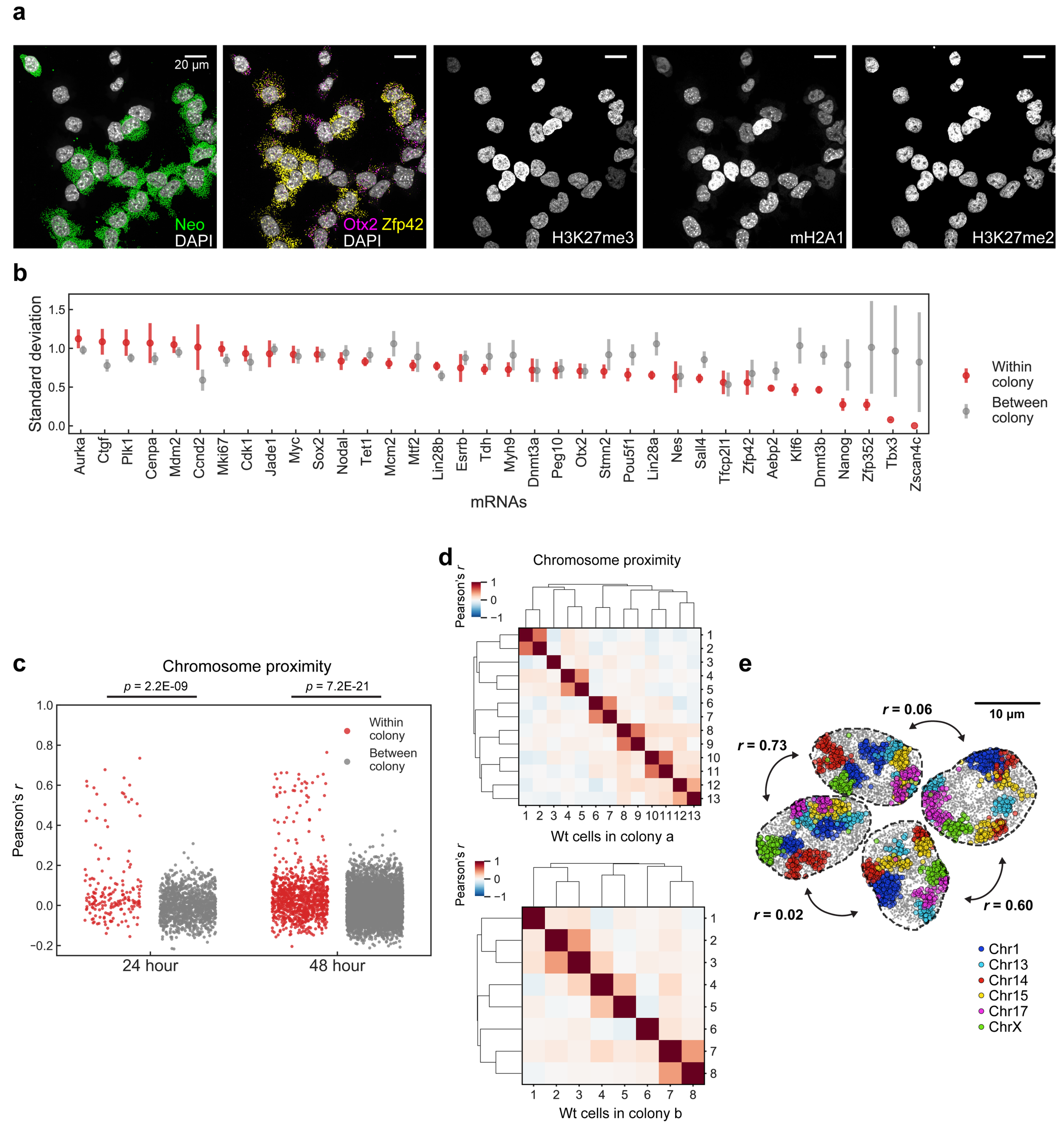

Extended Data Fig. 10 | Additional analysis for colony level cell state heterogeneity. a, mRNA and immunofluorescence images in a colony in the 48-h clonal tracing experiment. H3K27me3 and mH2A1 overall intensities are similar in WT cells (GFP/Neo negative) in the colony. **b**, Standard deviation of normalized mRNA levels within colonies (red) and between colonies (grey). Error bars show standard errors for 20 bootstrap trials. *Tbx3* and *Nanog* are more homogeneous within colonies, consistent with previous findings of the long-lived transcriptional states of these genes across several generations by single-cell live-imaging experiments[41,49]. $n = 117$ unlabelled cells within colonies from a 48-h dataset. **c**, Histogram of cell-to-cell correlations of chromosome to chromosome proximity maps for cells within colonies (red) and between colonies (grey). Cells with similar chromosome structures (red dots with high correlation values) are likely to be sister cells. The *y*-axis represents PCC, computed by 20 × 20 chromosome proximity matrices from pairs of cells. *P* values were from a two-sided Wilcoxon's rank-sum test with pairs of cells of 180, 1,198, 966 and 5,820 (left to right). **d**, Correlation of chromosome proximities between cells in colonies in the 48-h clonal tracing experiment. Strong correlations are seen between putative sister cells suggesting that gross chromosome proximities are preserved for one generation. Colour bars represent PCC computed in **c**. **e**, Chromosome images for unlabelled cells from a 24-h colony shows similarities between two sets of neighbouring cells (maximum *z*-projection). Chromosome organizations in single cells are highly correlated between pairs of cells that were physically close (possibly sister cells) and are mostly uncorrelated with other cells in the colonies. Six chromosomes are shown for visual clarity. *r* represents PCC computed in **c**.

nature research

Corresponding author(s): Cai

Last updated by author(s): 11/24/2020

Reporting Summary

Nature Research wishes to improve the reproducibility of the work that we publish. This form provides structure for consistency and transparency in reporting. For further information on Nature Research policies, see our Editorial Policies and the Editorial Policy Checklist.

Statistics

For all statistical analyses, confirm that the following items are present in the figure legend, table legend, main text, or Methods section.

n/a	Confirmed	
☐	☒	The exact sample size (n) for each experimental group/condition, given as a discrete number and unit of measurement
☐	☒	A statement on whether measurements were taken from distinct samples or whether the same sample was measured repeatedly
☐	☒	The statistical test(s) used AND whether they are one- or two-sided *Only common tests should be described solely by name; describe more complex techniques in the Methods section.*
☒	☐	A description of all covariates tested
☐	☒	A description of any assumptions or corrections, such as tests of normality and adjustment for multiple comparisons
☐	☒	A full description of the statistical parameters including central tendency (e.g. means) or other basic estimates (e.g. regression coefficient) AND variation (e.g. standard deviation) or associated estimates of uncertainty (e.g. confidence intervals)
☐	☒	For null hypothesis testing, the test statistic (e.g. F, t, r) with confidence intervals, effect sizes, degrees of freedom and P value noted *Give P values as exact values whenever suitable.*
☒	☐	For Bayesian analysis, information on the choice of priors and Markov chain Monte Carlo settings
☒	☐	For hierarchical and complex designs, identification of the appropriate level for tests and full reporting of outcomes
☐	☒	Estimates of effect sizes (e.g. Cohen's d, Pearson's r), indicating how they were calculated

Our web collection on statistics for biologists contains articles on many of the points above.

Software and code

Policy information about availability of computer code

Data collection	Custom written scripts in Micro-manager 1.4 for automated fluids delivery and image acquisitions.
Data analysis	Custom written scripts in MATLAB R2019a, Python (v3.8.3), Mathematica (v12.0), R (v3.6.3), PyMOL (v2.0) and ImageJ (v1.51s). In addition, following tools and algorithms were used, Bowtie2 (v2.3.1), Juicer tools (v1.5), Bedtools (v2.26.0), Seurat (v3.0), Cytoscape (v3.5.1), and 3D radial center algorithm (https://pages.uoregon.edu/raghu/particle_tracking.html). See the Methods section for the detail usages. The custom written scripts used in this study are available at https://github.com/CaiGroup/dna-seqfish-plus.

For manuscripts utilizing custom algorithms or software that are central to the research but not yet described in published literature, software must be made available to editors and reviewers. We strongly encourage code deposition in a community repository (e.g. GitHub). See the Nature Research guidelines for submitting code & software for further information.

Data

Policy information about availability of data

All manuscripts must include a data availability statement. This statement should provide the following information, where applicable:

- Accession codes, unique identifiers, or web links for publicly available datasets
- A list of figures that have associated raw data
- A description of any restrictions on data availability

Additional processed data from this study is available at Zenode website (DOI: 10.5281/zenodo.3735329). All raw data obtained during this study are available from the corresponding author upon reasonable request. Publicly available datasets used in the study (GSE96107, 4DNESOJRTZZR, GSE17051, GSE102076, GSE48895, ENCSR000CFN, ENCSR000CGP, ENCSR000CGQ) are detailed in the Methods.

Field-specific reporting

Please select the one below that is the best fit for your research. If you are not sure, read the appropriate sections before making your selection.

☒ Life sciences ☐ Behavioural & social sciences ☐ Ecological, evolutionary & environmental sciences

For a reference copy of the document with all sections, see nature.com/documents/nr-reporting-summary-flat.pdf

Life sciences study design

All studies must disclose on these points even when the disclosure is negative.

Sample size	Sample sizes were chosen to stabilize the measurement distributions. Analyses showing high reproducibility and the agreement of measurements with literatures (Shen et al. 2012; Hormoz et al. 2016; Bonev et al. 2017; Quinodoz et al. 2018) indicate that the sample sizes are sufficient. See Figure legends for each experiment.
Data exclusions	No raw data was excluded from the analysis. For downstream analysis, cells at the corner of the fields of view were excluded due to the laser illumination bias, and several antibodies (H3, H3K4me1, H3K4me2 and H3K4me3) were excluded due to the quality of antibody staining with oligo-conjugation.
Replication	Two independent biological replicates with hundreds of cells each were imaged. High Pearson's correlation coefficient of 0.92 for chromosome contact frequencies indicates the reproducibility of the methods between the two replicates.
Randomization	Individual cells across 5 to 10 different field of views were chosen randomly for image acquisition for each sample.
Blinding	No blinding was necessary for this study, and biological samples were defined before the measurements. Image processing and analyses were performed in an automated and identical way across different samples.

Reporting for specific materials, systems and methods

We require information from authors about some types of materials, experimental systems and methods used in many studies. Here, indicate whether each material, system or method listed is relevant to your study. If you are not sure if a list item applies to your research, read the appropriate section before selecting a response.

Materials & experimental systems

n/a	Involved in the study	
☐	☒	Antibodies
☐	☒	Eukaryotic cell lines
☒	☐	Palaeontology and archaeology
☒	☐	Animals and other organisms
☒	☐	Human research participants
☒	☐	Clinical data
☒	☐	Dual use research of concern

Methods

n/a	Involved in the study	
☒	☐	ChIP-seq
☒	☐	Flow cytometry
☒	☐	MRI-based neuroimaging

Antibodies

Antibodies used	mH2A1 (Abcam ab232602), E-Cadherin (R&D AF748), Fibrillarin (C13C3) (Cell Signaling 2639BF), Geminin (Abcam ab238988), GFP (Invitrogen G10362), H3 (Active Motif 39763), H3K27ac (Active Motif 39133), H3K27me2 (Cell Signaling 9728BF), H3K27me3 (Cell Signaling 9733BF), H3K4me1 (Cell Signaling 5326S), H3K4me2 (Cell Signaling 9725BF), H3K4me3 (Active Motif 39915), H3K9ac (Active Motif 91103), H3K9me2 (Abcam ab1220), H3K9me3 (Diagenode MAb-146-050), H3pSer10 (Millipore 05-806), H4K16ac (EMD Millipore 07-329), H4K20me1 (Abcam ab9051), H4K20me2 (Abcam ab9052), H4K20me3 (Active Motif 39671), Lamin B1 (Abcam ab220797), RNAPII Ser5-P (Abcam ab5408), SF3a66 (Abcam ab77800)
Validation	Localization patterns from oligo DNA conjugated antibodies were validated by comparing to those from unconjugated antibodies individually. All primary antibodies were purchased and validated by manufactures as follows. mH2A1 (Abcam ab232602) Application: Western Blot (WB), Immunohistochemistry (IHC-P), Immunocytochemistry (ICC)/Immunofluorescence (IF) Species reactivity: Mouse, Rat, Human E-Cadherin (R&D AF748) Application: WB, Simple Western, Flow Cytometry (Flow), IHC, CyTOF-ready, ICC Species reactivity: Human, Mouse

Fibrillarin (Cell Signaling 2639BF)
Application: WB, IF
Species reactivity: Human, Mouse, Rat, Monkey

Geminin (Abcam ab238988)
Application: IHC-P, WB, ICC/IF
Species reactivity: Human

GFP (Invitrogen G10362)
Application: ELISA, Flow, IHC, IP, WB
Species reactivity: Tag
Published species: C. elegans, Cat, Fruit fly, Human, Mouse, Non-human primate, Rat, Tag, Yeast, Zebrafish
The antibody is reported in the literature for IF application (list of publications on the manufacturer's website).

H3 (Active Motif 39763)
Application: Chromatin Immunoprecipitation (ChIP), ChIP-seq, IF, WB, ICC
Species reactivity: Human, Wide Range Predicted
The antibody is reported in the literature for Mouse reactivity (list of publications on the manufacturer's website).

H3K27ac (Active Motif 39133)
Application: ChIP, ChIP-seq, IF, WB, Dot Blot (DB), IHC, ICC
Species reactivity: Budding Yeast, Human, Wide Range Predicted
IF profiles obtained in this study were validated by ChIP-seq data (encodeproject.org, accession ENCSR000CGQ) in Extended Data Fig. 6a, b.

H3K27me2 (Cell Signaling 9728BF)
Application: WB, IP, IF, Flow, ChIP
Species reactivity: Human, Mouse, Rat, Monkey

H3K27me3 (Cell Signaling 9733BF)
Application: WB, IHC, IF, Flow, ChIP, CUT&RUN
Species reactivity: Human, Mouse, Rat, Monkey

H3K4me1 (Cell Signaling 5326S)
Application: WB, IF, Flow, ChIP
Species reactivity: Human, Mouse, Rat, Monkey

H3K4me2 (Cell Signaling 9725BF)
Application: WB, IP, IHC, IF, Flow, ChIP
Species reactivity: Human, Mouse, Rat, Monkey

H3K4me3 (Active Motif 39915)
Application: ChIP, ChIP-seq, WB, IF, DB, ICC
Species reactivity: Budding Yeast, Human, Wide Range Predicted
The antibody is reported in the literature for Mouse reactivity (list of publications on the manufacturer's website).

H3K9ac (Active Motif 91103)
Application: ChIP, ChIP-seq, WB, IF, ELISA, ICC
Species reactivity: Human, Wide Range Predicted
IF profiles obtained in this study were validated by ChIP-seq data (encodeproject.org, accession ENCSR000CGP) in Extended Data Fig. 6a, b.

H3K9me2 (Abcam ab1220)
Application: WB, ELISA, IHC-P, ChIP
Species reactivity: Rat, Chicken, Cow, Human, Xenopus laevis, Arabidopsis thaliana, Caenorhabditis elegans, Drosophila melanogaster, Schizosaccharomyces pombe, Corn, Common marmoset, Rice
Predicted species reactivity: Mouse, Sheep, Saccharomyces cerevisiae, Other species
The antibody is reported in the literature for IF application and Mouse reactivity (list of publications on the manufacturer's website).

H3K9me3 (Diagenode MAb-146-050)
Application: ChIP, DB, WB
Species reactivity: Human, Fungi
The antibody is reported in the literature for IF application and Mouse reactivity (list of publications on the manufacturer's website).

H3pSer10 (Millipore 05-806)
Application: Flow, ICC, IF, Platelet Immuno-Assay (PIA), WB, multiplexing (Mplex)
Species reactivity: Human
The antibody is reported in the literature for IF application and Mouse reactivity (list of publications on the manufacturer's website).

H4K16ac (EMD Millipore 07-329)
Application: WB, Mplex, PIA, DB, ChIP-seq, ChIP
Species reactivity: Human, Mouse, Rat
The antibody is reported in the literature for IF application (list of publications on the manufacturer's website).

H4K20me1 (Abcam ab9051)
Application: IHC-P, WB, ICC/IF, ChIP
Species reactivity: Mouse, Cow, Human

H4K20me2 (Abcam ab9052)
Application: IP, WB, ICC/IF, IHC-P
Species reactivity: Mouse, Cow, Schizosaccharomyces pombe, Toxoplasma gondii

H4K20me3 (Active Motif 39671)
Application: ChIP, WB, DB, ICC
Species reactivity: Human, Mouse, Wide Range Predicted

Lamin B1 (Abcam ab220797)
Application: ICC, IP, WB, IHC-P
Species reactivity: Mouse, Rat, Human
BSA and Azide containing batches (Abcam ab133741) are validated for IF by the manufacturer.

RNAPII Ser5-P (Abcam ab5408)
Application: Flow, ICC/IF, DB, ChIP, WB, ELISA
Species reactivity: Mouse, Rat, Human

SF3a66 (Abcam ab77800)
Application: IHC-P, WB, ICC/IF, Flow
Species reactivity: Rat, Human, Monkey
IF profiles obtained in this study were validated by SPRITE data (data.4dnucleome.org, accession 4DNESOJRTZZR) in Extended Data Fig. 6a, b.

Eukaryotic cell lines

Policy information about cell lines

Cell line source(s)	E14 mESCs (E14Tg2a.4) from Mutant Mouse Regional Resource Centers was used in this study.
Authentication	The cell lines were authenticated by DNA seqFISH+ (Extended Data Fig. 3a-g), multiplexed immunofluorescence (Extended Data Fig. 6a-f), and RNA seqFISH (Extended Data Fig. 9a-c), all of which gave results consistent with the embryonic stem cell identity.
Mycoplasma contamination	The cell line was not tested for mycoplasma contamination.
Commonly misidentified lines (See ICLAC register)	The cell line used was not listed in the ICLAC database.